Trojanowski JQ, Tomita T*, Iwatsubo T					
Miyashita H, Maruyama Y, Isshiki H, Osawa S, Ogura T, Mio K, Sato C, Tomita T*, Iwatsubo	Three dimensional structure of signal peptide peptidase.	J Biol Chem	286	26188-26197	2011
Ohki Y, Higo T, Uemura K, Shimada N, Osawa S, Funamoto S, Ihara Y, Berezovska O, Yokoshima S, Fukuyama T, Tomita T*, Iwatsubo T	Phenylpiperidine-type ◎-secretase modulators target the transmembrane domain 1 of presenilin 1.	EMBO J	30	4815-4824	2011
Yonemura Y, Futai E, Yagishita S, Suo S, Tomita T, Iwatsubo T, Ishiura S	Comparison of presenilin 1 and presenilin 2 ◎-secretase activities using a yeast reconstitution system.	J Biol Chem	52	44569-44575	2011
Hayashi I, Takatori S, Urano Y, Miyake Y, Takagi J, Sakata-Yanagimoto M, Iwanari H, Osawa S, Morohashi Y, Li T, Wong PC, Chiba S, Kodama T, Hamakubo T, Tomita T*, Iwatsubo T	Neutralization of the ◎-secretase activity by monoclonal antibody against extracellular domain of nicastrin.	Oncogene		In press	

Nishitsuji K, Hosono T, Uchimura K, Michikawa M.	Lipoprotein lipase is a novel Aβ-binding protein that promotes glycosaminoglycan-dependent cellular uptake of Aβ in astrocytes.	**J. Biol. Chem.**	**286**	6393-6401	2011
Nishitsuji K, Hosono T, Nakamura T, Bu G, Michikawa M.	Apolipoprotein E regulates the integrity of tight junctions in an isoform-dependent manner in an in vitro blood-brain-barrier model.	**J. Biol. Chem.**	286	17536-17542	2011
Yasuno F, Tanimukai S, Sasaki M, Hidaka S, Ikejima C, Yamashita F, Kodama C, Mizukami K, Michikawa M, Asada T	Association between cognitive function and plasma lipids of the elderly after controlling for apolipoprotein E genotype.	**Am. J. Geriat. Psychiat.**			
Takamura A, Kawarabayashi T, Yokoseki T, Shibata M, Morishima-Kawashima M, Saito Y, Murayama S, Ihara Y, Abe K, Shoji M, Michikawa M, Matsubara E	The dissociation of Aβ from lipoprotein in cerebrospinal fluid from Alzheimer's disease accelerates Aβ42 assembly.	**J. Neurosci. Res**	6	815-821,	2011
Takamura A, Okamoto Y, Kawarabayashi T, Yokoseki T, Shibata M, Mouri A, Nabeshima T, Sun H, Abe K,	Extracellular and intraneuronal HMW-Aβ oligomers represent a molecular basis of memory loss in Alzheimer's disease model mouse.	**Mol. Neurodegener**	6	20	2011

Shoji M, Yanagisawa K, Michikawa M, Matsubara E					
Akatsu H, Ogawa N, Kanesaka T, Hori A, Yamamoto T, Matsukawa N, Michikawa M.	Higher activity of peripheral blood angiotensin-converting enzyme is associated with later-onset of Alzheimer's disease.	**J. Neurol. Sci**	300	67-73	
Marutani T, Maeda T, Tanabe C, Zou K, Araki W, Kokame K, Michikawa M, Komano H.	ER-stress-inducible Herp, facilitates the degradation f immature nicastrin	**Biochim. Biophys. Acta**	1810	790-798	2011
H osono-Fukao T, Ohtake-Niimi S, Nishitsuji K, Hossain M, van Kuppevelt TH, Michikawa M, Uchimura K.	RB4CD12 epitope expression and heparan sulfate disaccharide composition in brain vasculature.	**J. Neurosci. Res.**	89	1840-1848	2011
Jung C-G, Uhm K-O, Miura Y, Hosono T, Horike H, Khanna K K, Michikawa M	Beta-amyloid increases the expression level of ATBF1 responsible for death in cultured cortical neurons	**Mol Neurodegener,**	6	47	2011

III.研究成果の刊行物・別刷

nature neuroscience

Potent amyloidogenicity and pathogenicity of Aβ43

Takashi Saito[1,8], Takahiro Suemoto[1,8], Nathalie Brouwers[2,3], Kristel Sleegers[2,3], Satoru Funamoto[4], Naomi Mihira[1], Yukio Matsuba[1], Kazuyuki Yamada[5], Per Nilsson[1], Jiro Takano[1], Masaki Nishimura[6], Nobuhisa Iwata[1,7], Christine Van Broeckhoven[2,3], Yasuo Ihara[4] & Takaomi C Saido[1]

The amyloid-β peptide Aβ42 is known to be a primary amyloidogenic and pathogenic agent in Alzheimer's disease. However, the role of Aβ43, which is found just as frequently in the brains of affected individuals, remains unresolved. We generated knock-in mice containing a pathogenic presenilin-1 R278I mutation that causes overproduction of Aβ43. Homozygosity was embryonic lethal, indicating that the mutation involves a loss of function. Crossing amyloid precursor protein transgenic mice with heterozygous mutant mice resulted in elevated Aβ43, impairment of short-term memory and acceleration of amyloid-β pathology, which accompanied pronounced accumulation of Aβ43 in plaque cores similar in biochemical composition to those observed in the brains of affected individuals. Consistently, Aβ43 showed a higher propensity to aggregate and was more neurotoxic than Aβ42. Other pathogenic presenilin mutations also caused overproduction of Aβ43 in a manner correlating with Aβ42 and with the age of disease onset. These findings indicate that Aβ43, an overlooked species, is potently amyloidogenic, neurotoxic and abundant *in vivo*.

© 2011 Nature America, Inc. All rights reserved.

Alzheimer's disease, the most common form of dementia, is characterized by two pathological features in the brain, extracellular senile plaques and intracellular neurofibrillary tangles. Senile plaques consist of amyloid-β peptide (Aβ) that is generated from amyloid precursor protein (APP) through sequential proteolytic processing by β-secretase and γ-secretase. Two major forms of Aβ exist, Aβ40 and Aβ42, with Aβ42 being more neurotoxic as a result of its higher hydrophobicity, which leads to faster oligomerization and aggregation[1]. A number of mutations associated with early-onset familial Alzheimer's disease (FAD) have been identified in the *APP*, *PSEN1* and *PSEN2* genes, and these mutations lead to accelerated production of Aβ42 or an increase in the Aβ42/Aβ40 ratio. Together, these findings indicate that Aβ42 is essential for the initiation of pathogenesis. However, the possible involvement of longer Aβ species that also exist in the brains of individuals with Alzheimer's disease has not yet been fully investigated.

Thus far, various longer Aβ species, such as Aβ43, Aβ45, Aβ48, Aβ49 and Aβ50, have been qualitatively described in the brains of individuals with Alzheimer's disease[2]. Similar Aβ species have also been found in transgenic mice that overexpress *APP* carrying FAD-linked mutations[3]. Further quantitative studies have revealed that Aβ43 is deposited more frequently than Aβ40 in both sporadic Alzheimer's disease (SAD) and FAD[4–7].

How these Aβ species with different C-terminal ends are generated from the precursor has mainly been investigated by cell biological and biochemical methods. A number of studies[8,9] have found that γ and ε cleavage by γ-secretase controls the fate of the C-terminal end. Aβ43, generated from Aβ49 via Aβ46, is subsequently converted to Aβ40 by γ-secretase, whereas Aβ42 is independently generated from Aβ48 via Aβ45. It has also been reported that the FAD-associated I213T mutation in the *PSEN1* gene increases the generation of longer Aβ species, such as Aβ43, Aβ45 and those even longer than Aβ46, in addition to Aβ42 (ref. 10). It is also noteworthy that Aβ43 appears to be as prone to aggregate *in vitro* as Aβ42 (ref. 11), leading to faster formation of oligomers than occurs in the case of Aβ40 (ref. 12). These observations imply that Aβ43 could be produced as a physiological or pathological metabolite of γ-secretase and may affect Aβ amyloidosis in the brain.

To address whether Aβ43 contributes to Alzheimer's disease pathology, we decided to take advantage of the molecular phenotype of the presenilin-1 (PS1) R278I mutation, as this mutation results in selective overt production of Aβ43 *in vitro*[13], an effect that occurs to a much greater extent than in the case of other mutations, such as R278K, R278S and R278T. The R278I mutation has been independently reported in a pedigree bearing atypical Alzheimer's disease with language impairment[14]. A follow-up survey revealed that one of the affected individuals subsequently progressed to more severe cognitive impairment, and another individual from a different branch of the family with the mutation showed Alzheimer's disease–associated symptoms with an early loss of episodic memory and with a clinical onset of the disease at 59 years of age (M.N. Rossor, University College London, personal communication).

[1]Laboratory for Proteolytic Neuroscience, RIKEN Brain Science Institute, Wako-shi, Saitama, Japan. [2]Neurodegenerative Brain Diseases Group, Department of Molecular Genetics, Flanders Interuniversity Institute for Biotechnology, Antwerpen, Belgium. [3]Laboratory of Neurogenetics, Institute Born-Bunge, University of Antwerp, Antwerpen, Belgium. [4]Faculty of Life Sciences, Doshisha University, Kyoto, Japan. [5]Research Resource Center, RIKEN Brain Science Institute, Wako-shi, Saitama, Japan. [6]Molecular Neuroscience Research Center, Shiga University of Medical Science, Shiga, Japan. [7]Department of Molecular Medicinal Sciences, Division of Biotechnology, Nagasaki University Graduate School of Biomedical Sciences, Nagasaki, Japan. [8]These authors contributed equally to this work. Correspondence should be addressed T.C.S. (saido@brain.riken.jp).

Received 17 March; accepted 13 May; published online 3 July 2011; doi:10.1038/nn.2858

We generated PS1-R278I knock-in mice to assess the biological importance of the mutation and the pathological effect of Aβ43 on Aβ amyloidosis. Homozygosity in knock-in mice was embryonic lethal, presumably because of a partial loss of γ-secretase activity that resulted in a failure in Notch1 processing. Consistent with this, mouse embryonic fibroblasts (MEFs) derived from the homozygous knock-in mice exhibited a failure in PS1 endoproteolysis and Notch1 processing, implying that the particular selectivity of the PS1-R278I mutation for Aβ43 production is closely associated with the partial loss of γ-secretase activity, that is, suppression of the Aβ43-to-Aβ40 conversion, which could also be caused by some of the other PS1 mutations. We crossed heterozygous knock-in mice with APP transgenic mice (APP23 mice carrying the human *APP* isoform 751 transgene harboring the Swedish mutation (K651N M652L)) and found that the progeny exhibited short-term memory loss before plaque formation and developed considerably accelerated amyloid pathology, indicating that Aβ43 is potently amyloidogenic and pathogenic *in vivo*.

RESULTS

Generation of PS1-R278I knock-in mice

To generate PS1 knock-in mice, we constructed a targeting vector carrying a point mutation that results in the replacement of arginine 278 to isoleucine in exon 8 of the *PSEN1* allele (**Supplementary Fig. 1a**). Homologous recombination, germline transmission and genotype were confirmed by Southern blotting and PCR (**Supplementary Fig. 1b,c**). The expression levels of the mutant and wild-type PS1 in the embryonic mouse brains were identical (**Supplementary Fig. 1d**). Unexpectedly, homozygous knock-in (R278I/R278I) was embryonic lethal at embryonic day 15–18 (E15–18; **Fig. 1a**). The mutant embryos showed an overall size reduction, a stubby tail, limb ateliosis and hemorrhage in the CNS as compared with wild-type littermate controls (**Fig. 1a**).

This phenotype is similar to that of PS1-deficient mice and Notch1-related mutant mice[15,16], although the adverse phenotype of the PS1-R278I knock-in mice appeared a few days later than that of PS1-deficient mice. In contrast, we observed no developmental deficits in heterozygous knock-in (+/R278I) mice (**Fig. 1a** and **Supplementary Fig. 2**). The lethal phenotype of the R278I mutation appears to be caused by a loss of developmental function that manifests only under the recessive condition. We generated two lines of double-mutant mice: R278I knock-in/PS1 knockout and M146V knock-in/PS1 knockout. The phenotype of former was embryonic lethal and the latter was normal (**Supplementary Fig. 3a–d**). This observation suggests that the R278 mutation is a loss-of-function mutation. To the best of our knowledge, this is the first case of developmental abnormality being caused by a FAD-linked PS1 point mutation.

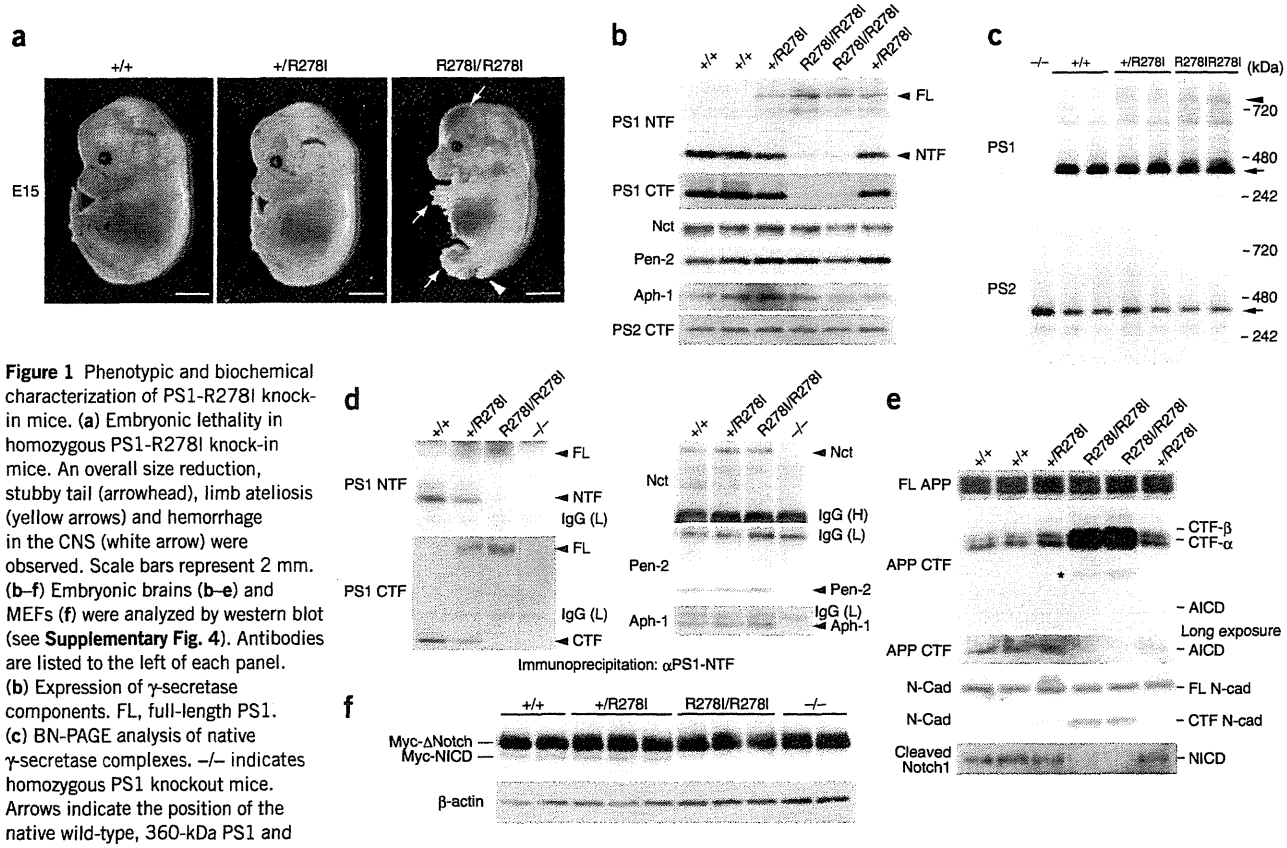

Figure 1 Phenotypic and biochemical characterization of PS1-R278I knock-in mice. (**a**) Embryonic lethality in homozygous PS1-R278I knock-in mice. An overall size reduction, stubby tail (arrowhead), limb ateliosis (yellow arrows) and hemorrhage in the CNS (white arrow) were observed. Scale bars represent 2 mm. (**b–f**) Embryonic brains (**b–e**) and MEFs (**f**) were analyzed by western blot (see **Supplementary Fig. 4**). Antibodies are listed to the left of each panel. (**b**) Expression of γ-secretase components. FL, full-length PS1. (**c**) BN-PAGE analysis of native γ-secretase complexes. –/– indicates homozygous PS1 knockout mice. Arrows indicate the position of the native wild-type, 360-kDa PS1 and PS2 γ-secretase complexes, whereas arrowhead points to the atypical high molecular weight (750 kDa) γ-secretase complex. (**d**) Immunoprecipitation by antibodies to PS1-NTF. IgG(H) and IgG(L) indicate immunoglobulin heavy and light chains, respectively. (**e**) γ-secretase activity in PS1-R278I knock-in brains. Brain extracts were analyzed by western blotting to detect endogenous APP CTF-β, APP CTF-α, APP intracellular domain (AICD), full-length N-cadherin, N-cadherin CTF and NICD products. * indicates an additional signal, smaller than that of CTF-α, which appeared in the knock-in mice. (**f**) Notch1 processing in PS1-R278I knock-in MEFs. Myc-tagged ΔNotch was transiently expressed in the MEFs, and cell lysates were subjected to western blot analysis using antibody to Myc. β-actin levels are shown as internal controls.

© 2011 Nature America, Inc. All rights reserved.

Abnormal PS1 endoproteolysis and Notch1 processing

To assess the functional importance of the R278I mutation in the PS1 knock-in line, we analyzed the biochemical properties of PS1-R278I γ-secretase in the embryonic brains before degeneration (**Fig. 1a**). Western blotting revealed a marked decrease in the levels of the N-terminal fragment (NTF) and C-terminal fragment (CTF) of PS1, indicating a failure of PS1 endoproteolysis, in homozygous knock-in brains, whereas the γ-secretase components, including Nicastrin (Nct), presenilin enhancer-2 (Pen-2) and anterior pharynx defective-1 protein (Aph-1), were expressed at normal levels (**Fig. 1b**). The NTF and CTF in the homozygous knock-in mice were, however, clearly detectable, indicating that a fraction of the endoproteolytic activity of PS1 still remained (**Fig. 1b** and **Supplementary Fig. 3e**). It is also noteworthy that the endoproteolysis was partially blocked in the heterozygous PS1-R278I brain, suggesting that the process is at least partly autolytic.

We next investigated whether the PS1-R278I mutation affects the assembly of the γ-secretase complex by Blue Native PAGE (BN-PAGE)[17]. A major signal corresponding to a molecular weight of 360 kDa, the normal molecular weight of the native PS1 γ-secretase complex, was detected in both wild-type and knock-in brains in a manner similar to that of the PS2 γ-secretase complex (**Fig. 1c**). Immunoprecipitation experiments further demonstrated that the mutant PS1 formed a complex with Nct, Pen-2 and Aph-1 (**Fig. 1d**). These data indicate that the PS1-R278I mutation does not affect the formation of the γ-secretase complex. Notably, BN-PAGE detected a minor signal corresponding to a higher molecular weight of 750 kDa in the homozygous knock-in brains (**Fig. 1c**). A similar higher molecular weight signal has been described in preparations from an individual with a deletion of exon 9 in the *PSEN1* gene (PS1-ΔE9)[17] and from SH-SY5Y cells treated with a γ-secretase inhibitor, L-685,458 (ref. 18). PS1-ΔE9 and PS1-ΔT440 also cause PS1 endoproteolytic abnormality in a similar manner to the PS1-R278I mutation[19–21]. The presence of this high molecular weight γ-secretase may reflect a conformational change in the multicomponent complex or binding of additional factor(s) to the complex, although its mechanistic involvement remains unclear.

We then examined the effect of the mutation on the metabolism of the γ-secretase substrates. Both the CTF-α and CTF-β of APP and the CTF of N-cadherin accumulated at substantial levels in the homozygous PS1-R278I knock-in mouse brain, but not in the wild-type or heterozygous brains (**Fig. 1e**). Conversely, the APP intracellular domain and Notch1 intracellular domain (NICD) could not be detected in the homozygous knock-in. An additional signal smaller than that of CTF-α appeared in the knock-in mice (**Fig. 1e**), presumably representing an aberrant proteolytic product of CTF-α and CTF-β. These data indicate that the PS1-R278I mutation leads to a substantial loss of γ-secretase activity in a recessive manner.

To further analyze the mutant γ-secretase, we established MEFs from knock-in mice and littermate controls. Western blotting (**Supplementary Fig. 4a**), BN-PAGE (**Supplementary Fig. 4b**) and immunoprecipitation experiments (**Supplementary Fig. 4c**) revealed that the biochemical properties of mutant presenilin in MEFs were

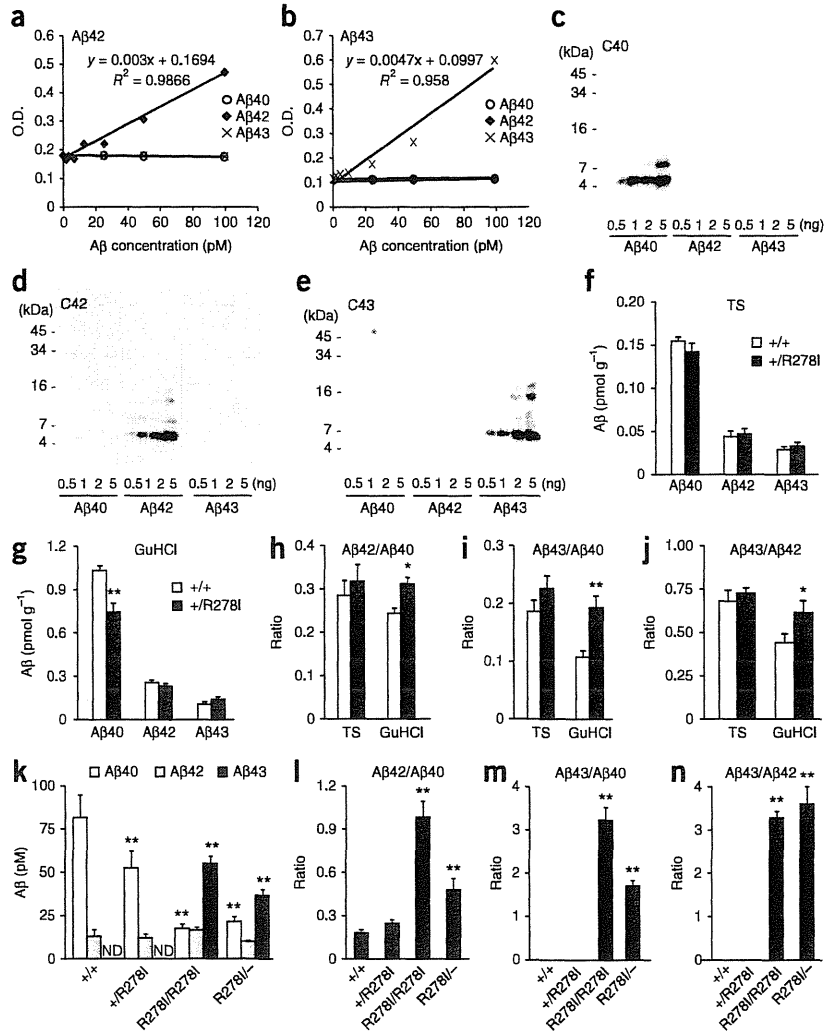

Figure 2 Aβ levels in adult PS1-R278I knock-in mouse brains and MEFs. (**a**,**b**) Establishment of ELISA system to specifically quantify Aβ42 and Aβ43 (see **Supplementary Figs. 6a**,**b** and **7**). (**c**–**e**) Specificity of the antibodies to Aβ40, Aβ42 and Aβ43 used in this ELISA system. Synthetic Aβ1–40, Aβ1–42 and Aβ1–43 were separated by tris/tricine PAGE (15% polyacrylamide gel) and subjected to western blotting. Antibodies to Aβ C40, C42 and C43 specifically recognized Aβ1–40, Aβ1–42 and Aβ1–43, respectively (see **Supplementary Fig. 6c–e**). (**f**–**n**) Quantification of Aβ40, Aβ42 and Aβ43 by ELISA in adult mouse brains (**f**–**j**) and MEFs (**k**–**n**). (**f**–**j**) Cortical hemispheres from 24-month-old wild-type and heterozygous knock-in mice were homogenized and fractionated into Tris-HCl–buffered saline–soluble (TS) and GuHCl-soluble fractions. Data represent mean ± s.e.m. ($n = 9$). $^*P < 0.05$ and $^{**}P < 0.01$ between wild-type and heterozygous knock-in mice, Student's t test. (**k**–**n**) Aβ concentrations in conditioned medium from MEFs. We inoculated 8×10^5 cells in a 1-ml culture. The conditioned medium was collected after 24 h and subjected to ELISA. R278I/– indicates a double heterozygote PS1-R278I knock-in × PS1 knockout mice. Data represent mean ± s.d. from two independent experiments ($n = 16$). $^{**}P < 0.01$ compared with wild type, one-way ANOVA with Scheffe's F test. ND, not detected.

© 2011 Nature America, Inc. All rights reserved.

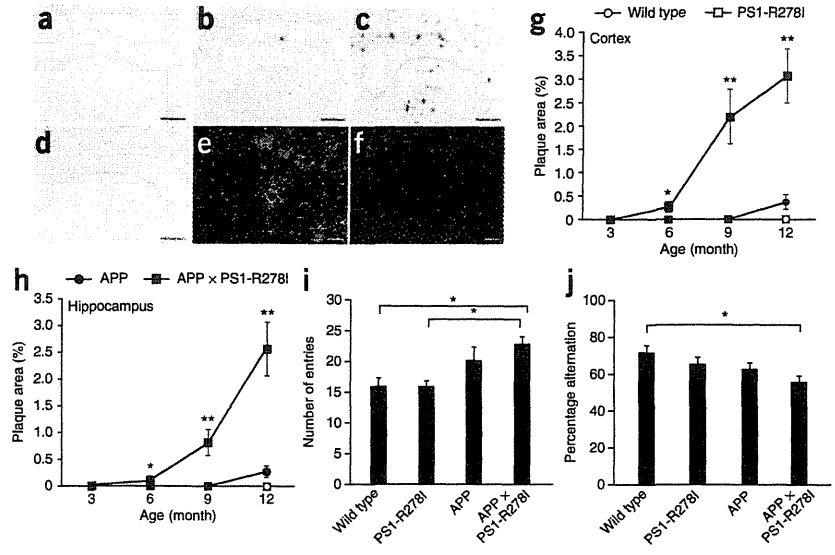

Figure 3 Acceleration of Aβ pathology and short-term memory impairment by the R278I knock-in mutation in APP mice. (**a–f**) Brain sections from APP × PS1-R278I mice (3 (**a**), 6 (**b**) and 9 months (**c**,**d**) old) and 9-month-old single APP mice (**d**,**f**) were immunostained with the 4G8 antibody to Aβ (**a–d**) and antibody to GFAP (green) with 4G8 counterstaining (red) (**e**,**f**). Aβ-immunostained brain sections from cortex (**g**) and hippocampus (**h**) of 3-, 6-, 9- and 12-month-old wild-type, APP and heterozygous PS1-R278I knock-in mice, as well as APP × PS1-R278I mice were analyzed ($n = 5$–6 each genotype). $^*P < 0.05$ and $^{**}P < 0.01$ compared with APP mice, two-way ANOVA with Scheffe's F test. Scale bars represent 500 μm (**a–d**) and 50 μm (**e**,**f**). (**i**,**j**) Y-maze test was performed before plaque formation using 3–4-month-old male wild-type, PS1-R278I knock-in, APP and APP × PS1-R278I mice. Data represent mean ± s.e.m. ($n = 10$ each genotype). $^*P < 0.05$ compared with wild-type or PS1-R278I knock-in mice, one-way ANOVA with Scheffe's F test.

identical to those in the embryonic brains. We then expressed Myc-tagged ΔNotch1 in the mutant and wild-type MEFs. Western blot analysis revealed that conversion of Myc-ΔNotch1 to Myc-NICD by limited proteolysis occurred in wild-type and heterozygous knock-in MEFs, but not in the homozygous knock-in or PS1 knockout MEFs (**Fig. 1f**). These results indicate that the R287I mutation induces developmental deficits by abolishing of γ-secretase–dependent Notch1 processing.

Aβ40, Aβ42 and Aβ43 in PS1-R278I knock-in brains and MEFs

Because homozygous R278I knock-in mice are embryonic lethal, we went on to analyze adult heterozygous knock-in mice. The adult heterozygous mice were normal in terms of development and anatomy at both 3 and 24 months of age (**Supplementary Fig. 2**), whereas various biochemical properties of PS1, such as partial abnormality of endoproteolysis, the molecular weight of γ-secretase and the identity of the complex components, were identical to those of the heterozygous embryonic brain (**Supplementary Fig. 5**). We then established a specific and highly sensitive ELISA system that could distinguish between Aβ40, Aβ42 and Aβ43 over a broad concentration range (**Fig. 2a,b** and **Supplementary Figs. 6a,b** and **7**). The antibodies that we used were highly specific to each Aβ species (**Fig. 2c–e** and **Supplementary Fig. 6c–e**). Brain tissue fractions that were soluble in Tris-HCl–buffered saline and those that were soluble in 6 M guanidine-HCl (GuHCl) were subjected to quantification.

There was a significant decrease in the steady-state levels of Aβ40 in the GuHCl-soluble fraction in the brains of aged (24 months old) heterozygous PS1-R278I knock-in mice as compared with wild-type animals ($P < 0.01$), although no differences were recorded in the levels of Aβs in the Tris-HCl–buffered saline fraction, or in the levels of Aβ42 and Aβ43 in the GuHCl-soluble fraction (**Fig. 2f,g**). This reduction of Aβ40 in the GuHCl-soluble fraction resulted in a significant elevation of the Aβ42/Aβ40 ($P < 0.05$) and Aβ43/Aβ40 ($P < 0.01$) ratios in the GuHCl-soluble fraction (**Fig. 2h,i**). Notably, the Aβ43/Aβ42 ratio was also significantly increased in the GuHCl-soluble fraction of the heterozygous PS1-R278I knock-in mouse brain ($P < 0.05$; **Fig. 2j**). In younger PS1-R278I knock-in mice (3 months old), Aβ43 levels were too low to detect, although the GuHCl-Aβ40 levels were again significantly reduced in the knock-in mice ($P < 0.05$; **Supplementary Fig. 8**). These results indicate that Aβ43 levels in the mouse brain increase on aging, and that the increase in the Aβ42/Aβ40 and Aβ43/Aβ40 ratios observed in the older heterozygous mice appears to be primarily caused by a decrease in Aβ40. Furthermore, the R278I mutation led to an elevation in the Aβ43/Aβ42 ratio in aged mice. Taken together, these findings indicate that the PS1-R278I mutation gives rise to a modest *in vivo* effect in terms of the levels of endogenous Aβ species under heterozygous conditions.

We next quantified the Aβ variants in conditioned medium from knock-in MEFs (**Fig. 2k–n**). The steady-state levels of Aβ40 were

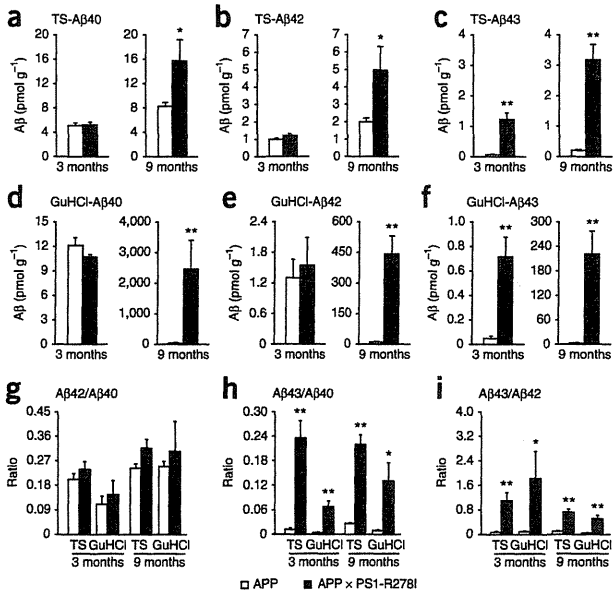

Figure 4 Aβ40, Aβ42 and Aβ43 in APP × PS1-R278I mice. (**a–i**) The levels of Aβ40 (**a**,**d**), Aβ42 (**b**,**e**) and Aβ43 (**c**,**f**) were quantified by ELISA and the ratios of the Aβ species (**g–i**) were subsequently determined. Cortical hemispheres from single APP and APP × PS1-R278I mouse brain (3 and 9 months old) were homogenized and fractionated into Tris-HCl–buffered saline–soluble fractions (**a–c**) and GuHCl-extractable fractions (**d–f**). Data represent mean ± s.e.m. ($n = 7$, 3 months old; $n = 5$, 9 months old). $^*P < 0.05$ and $^{**}P < 0.01$ between APP mice and APP × PS1-R278I mice, Student's t test.

© 2011 Nature America, Inc. All rights reserved.

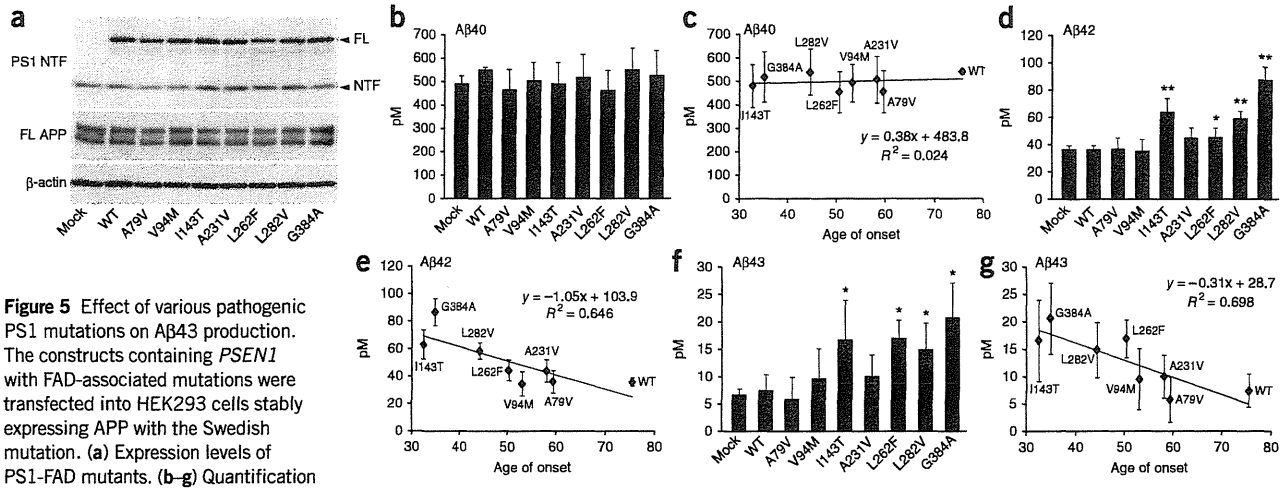

Figure 5 Effect of various pathogenic PS1 mutations on Aβ43 production. The constructs containing *PSEN1* with FAD-associated mutations were transfected into HEK293 cells stably expressing APP with the Swedish mutation. (**a**) Expression levels of PS1-FAD mutants. (**b–g**) Quantification of the steady-state levels of Aβ40, Aβ42 and Aβ43 and the correlation between Aβ levels and the age of disease onset. Age of onset is shown as follows: wild type (WT, 75 years old), A79V (59.3), V94M (53), I143T (32.5), A231V (58), L262F (50.3), L282V (44) and G384A (34.9)[24,44]. Data represent mean ± s.d. from five independent series each consisting of duplicate measurements. $*P < 0.05$ and $**P < 0.01$ compared with wild type, one-way ANOVA with Dunnett test.

© 2011 Nature America, Inc. All rights reserved.

significantly reduced in a gene dose–dependent manner in the PS1-R278I MEFs as compared with wild-type MEFs ($P < 0.01$). In contrast, Aβ43 markedly increased in the homozygous knock-in MEFs, whereas Aβ42 levels remained unchanged in all genotypes (**Fig. 2k**). Thus, the ratios of longer Aβ species significantly increased in homozygous PS1-R278I knock-in MEFs ($P < 0.01$; **Fig. 2l–n**). Notably, there was no increase in Aβ43 levels in conditioned medium from heterozygous knock-in MEFs (**Fig. 2k**). To unravel the underlying mechanism, we crossed heterozygous R278I knock-in mice with PS1 knockout mice (R278I/−) and measured the levels of Aβs present in conditioned medium from cultured MEFs. Aβ43 levels were increased, implying that wild-type PS1 processes Aβ43 to Aβ40 in heterozygous PS1-R278I knock-in MEFs (**Fig. 2k**). Furthermore, no Aβ43 was detected in heterozygous PS1 knockout MEFs (data not shown). Together, the data suggests that the γ-secretase substrate can be transferred between separate PS1 molecules or between dimers of PS1, as previously suggested[22], or even between PS1 molecules in the PS1 complexes, for further processing. The fact that total Aβ (Aβ40 + Aβ42 + Aβ43) was decreased in heterozygous knock-in MEFs, as compared with homozygous knock-in MEFs, is of particular interest. This might be a result of a dysfunctional PS1 heterodimer, with wild-type PS1 being either directly affected by PS1-R278I or overloaded with Aβ43 generated by PS1-R278I. Further experiments are required to resolve the reason behind the decreased total Aβ level (**Fig. 2k** and **Supplementary Fig. 9b**). Taken together, our data indicate that the R278I mutation

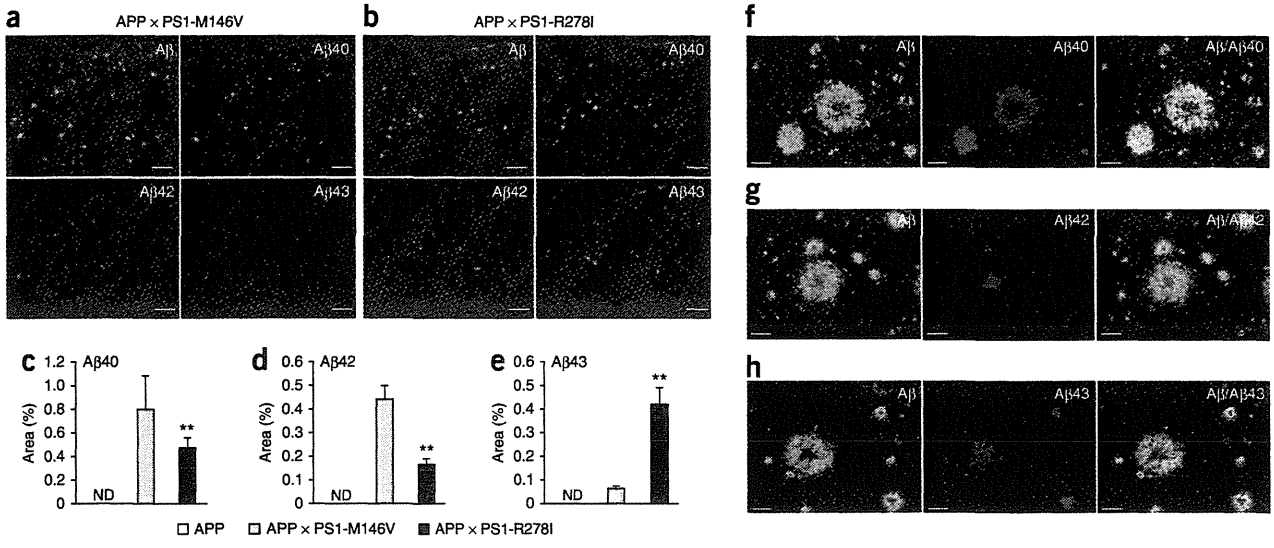

Figure 6 Localization of Aβ species in amyloid plaques of APP × PS1-R278I mice. (**a,b**) A set of serial brain sections from 9-month-old APP × PS1-M146V mice (**a**) and APP × PS1-R278I mice (**b**) were immunostained with the following antibodies to Aβ: 4G8 (total Aβ), C40 (Aβ1–40), C42 (Aβ1–42) and C43 (Aβ1–43). (**c–e**) The immunoreactive areas in single APP (left), APP × PS1-M146V (middle) and APP × PS1-R278I (right) mice were quantified as indicated ($n = 6$). $**P < 0.01$ between APP × PS1-M146V mice and APP × PS1-R278I mice, one-way ANOVA with Scheffe's F test. ND, not detected. (**f–h**) Double-staining with 4G8 (green) and Aβ40 (**f**), Aβ42 (**g**) or Aβ43 (**h**) (red). The images in the left (green) and middle (red) are merged (yellow) on the right. Scale bars represent 500 μm (**a,b**) and 50 μm (**f–h**).

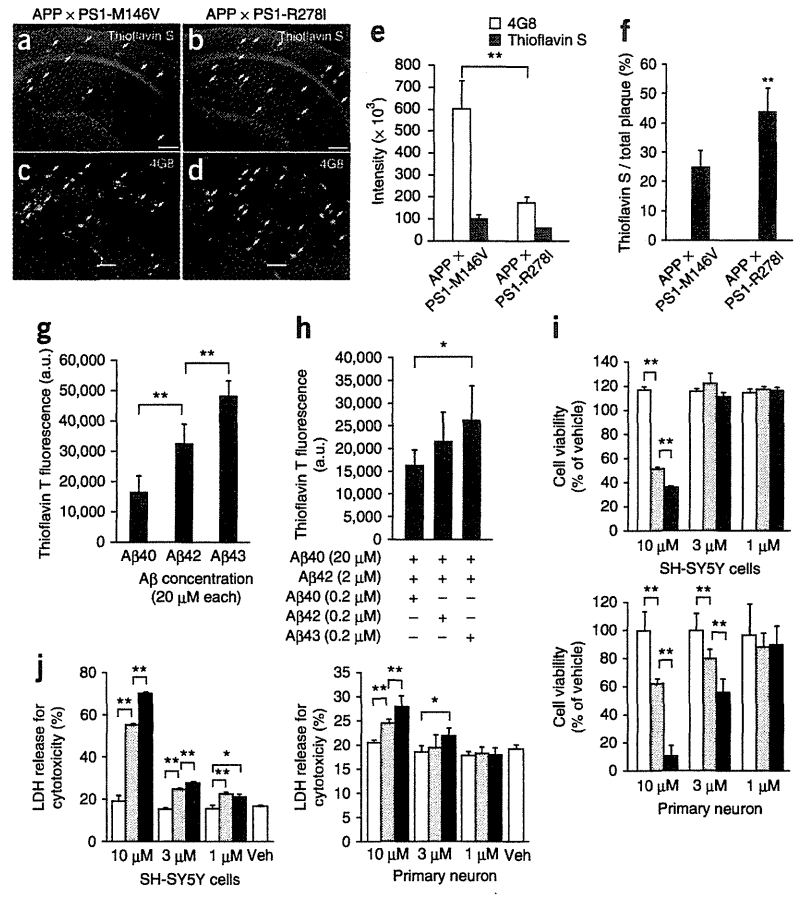

Figure 7 Mature amyloid plaques in APP × PS1-R278I mice and *in vitro* aggregation property and neural cell toxicity of Aβ43. (**a–f**) A set of serial brain sections from 9-month-old APP × PS1-M146V mice (**a**,**c**) and APP × PS1-R278I mice (**b**,**d**) were stained with thioflavin S (**a**,**b**) and immunostained with 4G8 (**c**,**d**). Thioflavin S–positive plaque are marked with arrows (**a**,**b**) and the corresponding plaques in the serial brain sections are also marked (**c**,**d**). Scale bars represent 500 μm. (**e**,**f**) The intensity of cortical and hippocampal Aβ immunoreactivity and thioflavin S signals were quantified (**e**), and the ratio of thioflavin S/total Aβ signal of amyloid plaques was determined (**f**) ($n = 12$). Data represent mean ± s.e.m. $^{**}P < 0.01$ between APP × PS1-M146V mice and APP × PS1-R278I mice, Student's *t* test. (**g**,**h**) *In vitro* Aβ aggregation experiments. Incorporation of thioflavin T into Aβ aggregates was measured by fluorescence spectroscopy. The aggregation properties of 20 μM Aβ40, Aβ42 and Aβ43 at 20 μM were measured individually in **g**. The effect of Aβ40, Aβ42 and Aβ43 at a concentration of 0.2 μM on the mixture of 20 μM Aβ40 and 2 μM Aβ42 was then assessed in **h**. Data represent mean ± s.d. from three independent series each consisting of 6–8 individual measurements. $^{**}P < 0.01$ between Aβ40 and Aβ42 or between Aβ42 and Aβ43, $^{*}P < 0.05$ between Aβ40 and Aβ43, one-way ANOVA with Scheffe's *F* test. (**i**,**j**) Neural cell toxicity of Aβ43. Cell viability (**i**) and lactate dehydrogenase (LDH) release as a measure of cell toxicity (**j**) were assayed. Aβs were administrated at 1, 3 and 10 μM, respectively. The results obtained after treatment with Aβ40 (white), Aβ42 (gray) and Aβ43 (black) are indicated, and vehicle (veh) treatment was also indicated by open column in (**j**). Data represent mean ± s.d. from three independent series each consisting of six individual measurements. $^{**}P < 0.01$ between Aβ40 and Aβ42 or between Aβ42 and Aβ43, and $^{*}P < 0.05$ between Aβ40 and Aβ43, two-way ANOVA with Scheffe's *F* test or Dunnett test.

© 2011 Nature America, Inc. All rights reserved.

inhibits Aβ43 to Aβ40 conversion, leading to increased Aβ43 levels and concomitant decrease of Aβ40 without altering Aβ42 levels. A similar Aβ-processing pathway has been described previously[9] (**Fig. 2k** and **Supplementary Fig. 10**).

Aβ pathology and memory impairment of APP mice

Overexpression of wild-type human APP in the above-stated MEFs using a semliki-forest virus vector[23] resulted in a significant increase in Aβ43 in the heterozygous R278I knock-in cells ($P < 0.05$; **Supplementary Fig. 9**). The presence of the excessive γ-secretase substrates, that is, APP CTF-α and CTF-β, appeared to force the mutant PS1 to participate in APP processing. These observations prompted us to crossbreed heterozygous PS1-R278I knock-in mice with APP mice to assess the effect of Aβ43 *in vivo*. APP × PS1-R278I mice started to accumulate pathological Aβ deposits at around 6 months of age, whereas it took about 12 months for APP transgenic mice to begin to show signs of such deposition (**Fig. 3a–h**). Massive astrocytosis was also detected around the amyloid plaques by 9 months age in the APP × PS1-R278I mice, but not in single transgenic mice (**Fig. 3e,f**). Behaviorally, 3–4-month-old APP × PS1-R278I mice exhibited short-term memory impairment as compared with single transgenic mice when their performance was evaluated in a Y-maze test (**Fig. 3i,j**). A similar tendency was also observed in the Morris water-maze test, although the difference in this case did not reach statistical significance ($P = 0.051$; data not shown). Taken together, these findings indicate that the PS1-R278I mutation leads to accelerated Aβ pathology with an accompanying inflammatory response and that the cognitive impairment occurs even before plaque formation.

We next quantified the steady-state levels of Aβ40, Aβ42 and Aβ43 in the brains of APP and APP × PS1-R278I mice at 3 and 9 months. Notably, only the double-mutant mice exhibited selective elevation of Aβ43 in both Tris-HCl–buffered saline–soluble and GuHCl-soluble brain fractions at 3 months, which is a time before the pathological deposition of Aβ (**Fig. 4a–f**), but by which the double-mutant mice already showed short-term memory impairment (**Fig. 3i,j**). In contrast, Aβ40 and Aβ42 levels started to increase at around 9 months. Consequently, both the Aβ43/Aβ40 and Aβ43/Aβ42 ratios were higher in the double mutant mice than in the single APP transgenic mice at both 3 and 9 months, whereas the Aβ42/Aβ40 ratio remained unaltered (**Fig. 4g–i**). It is worth noting that the elevation of biochemically detectable Aβ43 levels preceded plaque formation, implying that Aβ43 may be the initial seeding species and the trigger of memory impairment in this mouse model. The steady-state level of Aβ43 also increased in an age-dependent manner in the single APP transgenic mouse brains, beginning before plaque formation (**Fig. 3g,h** and **Supplementary Fig. 11**).

In addition, we observed that a variety of FAD-associated PS1 mutations resulted in overproduction of Aβ43 in a manner correlating with

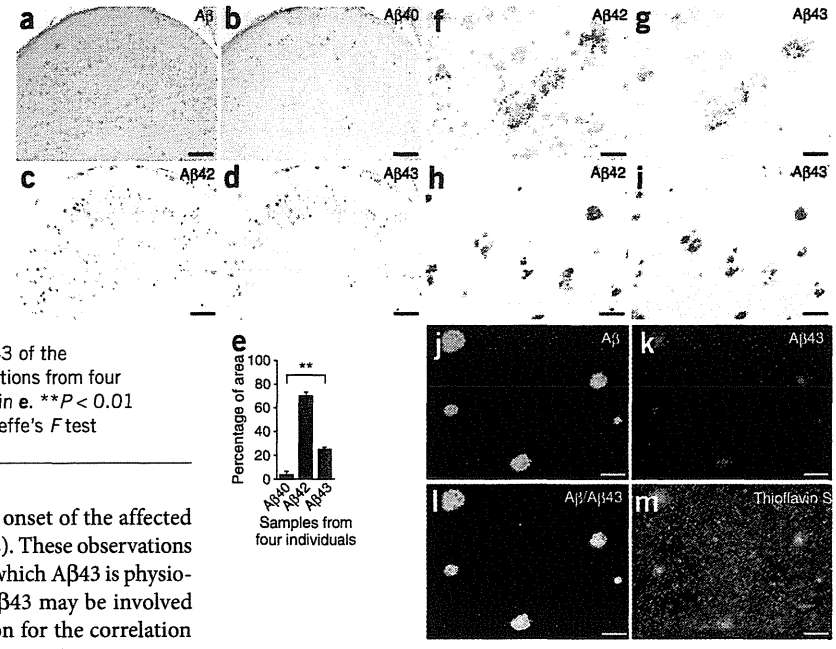

Figure 8 Aβ43 in amyloid plaques in Alzheimer's disease brains. (**a–m**) Serial sections of the hippocampal region (**a–d,h,i,j–m**) and the frontal cortical region of brains from individuals with Alzheimer's disease (**f,g**) were stained with 4G8 (total Aβ), C40 (Aβ1–40), C42 (Aβ1–42) and C43 (Aβ1–43), as well as thioflavin S, as indicated. The single staining (**a–d,f–i**) was developed using 3,3′-diaminobenzidine, whereas the double staining (**j–m**) used the fluorescent dyes fluorescein (green, Aβ) and rhodamine (red, Aβ43). The images in **j** and **k** are merged (yellow) in **l**. Scale bars represent 250 μm (**a–d**) and 25 μm (**f–m**). The ratio of Aβ40, Aβ42 and Aβ43 of the plaque areas in the hippocampal region of brain sections from four individuals with Alzheimer's disease were quantified in **e**. $^{**}P < 0.01$ between Aβ40 and Aβ43, one-way ANOVA with Scheffe's *F* test (see **Supplementary Fig. 15**).

the quantity of Aβ42 as well as with the age of onset of the affected individuals[24] (**Fig. 5** and **Supplementary Fig. 12**). These observations suggest that there is an intrinsic mechanism by which Aβ43 is physiologically generated and that both Aβ42 and Aβ43 may be involved in Alzheimer's disease pathogenesis. The reason for the correlation between Aβ42 and Aβ43 remains elusive.

APP × PS1-R278I versus APP × PS1-M146V mice

We generated another line of double-mutant mice by crossbreeding the APP transgenic mice with PS1-M146V knock-in mice, which served as a positive control with which to compare the APP × PS1-R278I mice, as the former mutation results in overproduction of Aβ42 rather than Aβ43 (ref. 25). As expected, the PS1-M146V mutation, unlike the PS1-R278I mutation, resulted in selective accumulation of Aβ42 (**Supplementary Fig. 13**). Although the steady-state levels of Aβ42 in the APP × PS1-M146V mice was about tenfold greater than that of Aβ43 in APP × PS1-R287I mice at 9 months, the total plaque areas, as determined by immunohistochemistry, were similar (**Fig. 6**). Both double-mutant mice accumulated Aβ40 and Aβ42, whereas Aβ43 was much more abundant in the APP × PS1-R278I mice (**Fig. 6a,b**). Quantitative image analyses yielded consistent results (**Fig. 6c–e**). Aβ43 immunoreactivity colocalized with the plaque cores in a manner similar to that of Aβ42, but not to that of Aβ40 (**Fig. 6f–h**). Notably, Aβ species with the third N-terminal residue converted to pyroglutamate (N3pE-Aβ), a potently pathogenic Aβ subspecies[26–29], also colocalized with plaque cores and deposits were more abundant in APP × PS1-R278I than in APP × PS1-M146V mice (**Supplementary Fig. 14**). Although the underlying mechanism that accounts for the elevated N3pE-Aβ generation in the APP × PS1-R278I mice remains unclear, the observation is consistent with a previous finding that some presenilin mutations increase the quantity of N-terminally truncated Aβ in the brains of individuals with FAD[30].

Although APP × PS1-M146V mice accumulated greater numbers of Aβ plaques in the cortical and hippocampal areas than APP × PS1-R278I mice, the density of thioflavin S–positive plaques per total plaques was significantly greater in the APP × PS1-R278I mice ($P < 0.01$; **Fig. 7a–f**). This observation indicates that Aβ43 is even more prone to seed cores in plaque formation than Aβ42. To test this hypothesis *in vitro*, we carried out thioflavin T–binding experiments using an equal amount of Aβ40, Aβ42 and Aβ43 (20 μM each). Aβ43 induced the highest incorporation of thioflavin T into Aβ aggregates (**Fig. 7g**). In addition, stoichiometric experiments, in which we added a relatively small quantity of Aβ40, Aβ42 or Aβ43 (0.2 μM) to a mixture of Aβ40 (20 μM) and Aβ42 (2 μM), revealed that, of the three, Aβ43 most potently accelerated the incorporation of thioflavin T (**Fig. 7h**). These data indicate that Aβ43 contributes to the formation of the thioflavin T–positive β-sheeted structure to a greater extent than either Aβ40 or Aβ42, a finding that may account for the observation that a relatively small amount of Aβ43 is sufficient to accelerate Aβ amyloidosis and induce plaque core formation *in vivo*.

Neural toxicity and amyloid pathology of Aβ43

Consistent with Aβ42 having higher hydrophobicity and higher toxicity than Aβ40 *in vitro* and *in vivo*, a large number of studies have found that Aβ42 contributes to synaptic dysfunctions[31–34]. We therefore compared the toxicity of Aβ40, Aβ42 and Aβ43. Aβ43 showed a higher potent neural toxicity in a dose-dependent manner as compared with Aβ40 and Aβ42 (**Fig. 7i,j**). These results indicate that Aβ43 directly affects neural toxicity and induces synaptic dysfunction, which would contribute to short-term memory impairments before the amyloidogenesis (**Fig. 3i,j**).

Finally, we performed immunohistochemical experiments on brain sections from individuals with SAD to explore the possible involvement of Aβ43 in human neuropathology. Aβ43 accumulated in the brains more frequently than Aβ40 (**Fig. 8a–e** and **Supplementary Fig. 15**), and was present in both diffuse (**Fig. 8f,g**) and dense-cored (**Fig. 8h,i**) plaques, similar to Aβ42 and N3pE-Aβ (**Supplementary Fig. 16a–d**). Furthermore, thioflavin S fluorescence signals colocalized well with Aβ43 immunoreactivity (**Fig. 8j–m**), as well as with N3pE-Aβ (**Supplementary Fig. 16e–g**). These observations are consistent with those of previous studies, which found that a substantial amount of Aβ43 accumulates in SAD and FAD brains[4–7].

DISCUSSION

Previous studies using Bri-Aβ fusion proteins have shown that Aβ42 is essential for amyloid deposition *in vivo*[31] and that Aβ40 inhibits this deposition[32]. The difference between Aβ40 and Aβ42 lies in the C-terminal amino-acid sequence, that is, the additional presence of isoleucine and alanine residues in Aβ42. Because both isoleucine and alanine are hydrophobic amino acids, it is reasonable to assume

© 2011 Nature America, Inc. All rights reserved.

that Aβ42 is more prone to form a β-sheet structure than Aβ40. In contrast, the carboxyl-terminal amino acid of Aβ43 is threonine, which carries a hydrophilic alcohol group (together with a hydrophobic methyl group) and could therefore reverse the hydrophobicity of Aβ42. Thus, the amyloidogenicity of Aβ43, a natural product of γ-secretase activity[8,9], has remained elusive.

We focused on Aβ43, an overlooked species in Alzheimer's disease research, and investigated its role in the amyloidogenesis and pathogenesis of Alzheimer's disease. To date, the major focus of research into Alzheimer's disease has been placed on the amyloidogenecity of Aβ42 and, in numerous studies, BC05, an antibody to Aβ42 that has been used to demonstrate that Aβ42 is the major pathogenic species in Alzheimer's disease. As partial crossreactivity of BC05 to Aβ43 had already been reported[35], Aβ42(43) was noted in some of the studies that used BC05. However, many studies have overestimated Aβ42 levels and ignored the possible changes in Aβ43 levels. Almost all FAD-associated PS1 mutations result in an increased Aβ42/Aβ40 ratio that is caused by an increase of Aβ42. However, some of the PS1 mutations lead to a decrease of Aβ40 with or without alteration of Aβ42 levels, which also leads to an increased Aβ42/Aβ40 ratio. One explanation of the association between decreased Aβ40 and FAD could be that Aβ40 is involved in protection from plaque fromation[32]. We found that decreased Aβ40 levels accompanied increased Aβ43 levels in PS1-R278I knock-in mice. Furthermore, the increased Aβ43 levels accelerated Aβ pathology, contributing to the early onset of the disease. Thus, we propose that Aβ43 should be separately analyzed from Aβ42.

In an effort to explore the role of Aβ43 in Aβ amyloidosis, we generated PS1-R278I knock-in mice, as this mutation causes overproduction of Aβ43 *in vitro*[13]. We chose to use this presenilin mutation knock-in procedure rather than the overexpression strategy for the following reasons. First, the R278I mutation is known to be clinically pathogenic. Second, the knock-in procedure is less artificial than transgenic overexpression approaches in general, and the knock-in mice could potentially be used to generate a relevant Alzheimer's disease model by crossbreeding with other mice, such as mutant APP transgenic or knock-in mice. Unexpectedly, the phenotype of the homozygous knock-in mice proved to be embryonic lethal in association with abnormal PS1 endoproteolysis. Limited proteolysis of APP CTF-α and CTF-β, N-cadherin, and Notch1 was also hampered in the homozygous knock-in embryos, although the γ-secretase components appeared to have been properly assembled as a 360-kDa complex. On the basis of previous studies, it appears that the disturbance in Notch1 processing represents the primary cause of the premature death that we observed[16,36]. Compared with PS1 knockout, the embryonic lethality of PS1-R278I knock-in mice occurs at a slightly later stage. Taking into account the fact that a 50% reduction of γ-secretase activity in heterozygous PS1-R278I or in heterozygous PS1 knockout mice does not lead to embryonic lethality and that a 90% reduction in homozygous PS1-R278I mice is lethal, it seems that the γ-secretase activity threshold for survival is somewhere between 10–50% of wild type. The remaining 10% γ-secretase activity in homozygous PS1-R278I knock-in mice could account for the delayed lethality compared with PS1 knockout mice (**Supplementary Fig. 10c**). Taken together, these results strongly suggested that the primary phenotype of the R278I mutation was a partial loss of function of γ-secretase activity.

Despite this, MEFs prepared from homozygous embryos produced extremely high steady-state levels of Aβ43 (approximately 20-fold greater than that of wild-type MEFs); this accompanied a substantial decrease in Aβ40 production and no changes in Aβ42 levels. Previous *in vitro* studies have found that Aβ43 is processed to Aβ40, whereas Aβ42 is independently produced from Aβ45 in the presence of γ-secretase[8,9]. Consistent with these findings, our results from crossbreeding heterozygous PS1-R278I mice with PS1 knockout mice, which showed substantial levels of both Aβ40 and Aβ43, indicate that Aβ43 was indeed converted to Aβ40 independently of Aβ42 production (**Fig. 2k**). Furthermore, we carried out *in vitro* γ-secretase assays and found that the ratio of production of Aβ46 in homozygous PS1-R278I MEFs was increased with a concomitant increase of Aβ43 and decrease of Aβ40 (**Supplementary Fig. 10**), suggesting that production of Aβ40 and Aβ43 also depends on Aβ46 production, as previously postulated[8–10]. Thus, inhibition of this Aβ43-to-Aβ40 conversion could account for the increase in Aβ43 and the concomitant decrease in Aβ40 in the knock-in MEFs. Notably, treatment of PS1-ΔE9–expressing cells with L-685,458 results in elevated Aβ43 production[37], consistent with the notion that multiple processes are involved in the generation of various Aβ species and that a partial loss of γ-secretase activity might give rise to a particular Aβ species. However, *in vitro* γ-secretase activity of heterozygous and homozygous PS1-R278I was markedly reduced in a gene dose–dependent manner, whereas there were no substantial differences in the steady-state levels of total MEF-produced Aβ compared with wild-type MEFs. To elucidate the reason behind this contradiction, it will be necessary to investigate other mechanisms, such as intracellular trafficking and secretion of Aβ, in depth.

The molecular mechanism that allows Aβ43 production, but not other proteolytic processes, remains to be clarified, but it likely involves specific conformational changes of the γ-secretase complex[38]. Because Aβ42 is produced independently of Aβ43 in the presence of γ-secretase, some of the FAD-associated PS1 mutations that cause a decrease in Aβ40 without an increase in Aβ42, such as A79V, A231V, C263F, L282V, L166P and G384A[24,39], might actually result in the elevation of Aβ43 in a manner similar to the R278I mutation. In addition, PS1-ΔE10, an artificial PS1 mutation located to the loop domain of PS1 where R278I is present, leads to a substantial reduction of the steady-state levels of Aβ40 without any alteration of Aβ42 levels, similar to our results; however, Aβ43 levels were not measured[40]. It will therefore be important to investigate whether these FAD-associated mutations give rise to increased Aβ43 levels and to scrutinize their amyloidogenicity. In fact, the I143T, L262F, L282V and G384A mutations did lead to substantial production of Aβ43 in our transfection assays. Notably, Aβ43 levels and the ratio of Aβ43/Aβ40 substantially correlated well with the age of disease onset in a manner similar to Aβ42 levels and the ratio of Aβ42/Aβ40. In addition, a PS1-I143T carrier in a Swedish family with FAD gave rise to high levels of Aβ43 (ref. 7). These observations highlight the possibility that compounds that facilitate the Aβ43-to-Aβ40 and Aβ42-to-Aβ38 conversions might be beneficial for prevention and treatment of Alzheimer's disease by decreasing both Aβ42 and Aβ43. In support of this notion, an oral vaccination with an adeno-associated virus vector carrying Aβ1–43 cDNA was reported to result in a marked reduction of Aβ burdens and improvement of behavioral performances in Tg2576 APP transgenic mice[41,42].

Although we originally thought to generate APP × homozygous PS1-R278I mice, we also explored the possible utility of heterozygous PS1-R278I knock-in mice, given that overexpression of APP in heterozygous PS1-R278I knock-in MEFs resulted in selective elevation of Aβ43. Consistent with this, APP × heterozygous PS1-R278I mice exhibited short-term memory impairment, selective biochemical accumulation of Aβ43 at an early stage before plaque formation and substantial acceleration of Aβ pathology thereafter as compared with APP mice. It should also be noted that the APP × PS1-R278I mice

© 2011 Nature America, Inc. All rights reserved.

exhibited a greater density of the thioflavin S–positive signal per plaque than APP × PS1-M146V mice, which overproduced Aβ42 instead of Aβ43. Consistent with previous reports[6,7], we observed Aβ43-positive plaques more often than Aβ40-positive ones in the brains of individuals with Alzheimer's disease. Aβ43 has previously been found in amyloid plaques in individuals with Alzheimer's disease[4,6,7], as well as in aged gorillas[43] and in some Alzheimer's disease model mice harboring PS1 or APP FAD mutations[3,10]. In addition, it has been suggested that the amount of Aβ43 in plaques correlates with cognitive decline[5]. We also found that Aβ43 exhibited potent neural toxicity, comparable to or even greater than that of Aβ42. These findings establish that Aβ43 is indeed amyloidogenic *in vivo* and likely to be pathogenic. Thus, the C-terminal amino acid residue of Aβ43, threonine, appears to strengthen the hydrophobicity of the peptide rather than reversing it.

Notably, biochemical accumulation of Aβ43 preceded pathological deposition in the APP × PS1-R278I mice and in the single APP mice. In addition, the basal Aβ43 levels substantially increased with aging in wild-type mice up to at least 18 months of age (data not shown). These observations suggest that Aβ43 is potentially valuable as a biomarker for presymptomatic diagnosis of Alzheimer's disease. We believe that it would be worth trying to quantify Aβ43 levels in cerebrospinal fluid from individuals with Alzheimer's disease and controls. We also detected the presence of N3pE-Aβ in APP × PS1-R278I mouse brains, a finding that is supported by a previous report quantitatively describing N3pE-Aβ42 and N3pE-Aβ43 in the brains of individuals with FAD or SAD[2]. It is of particular interest that Pittsburgh Compound B, a probe for amyloid imaging by positron emission tomography, selectively binds to N3pE-Aβ[26], implying that N3pE-Aβ42/43 could be particularly prone to seed deposition of other Aβ species, consistent with previous findings[28]. It is also possible that the mutation might affect the interaction of PS1 with other substrates or alter its property of non-γ-secretase activity, such as regulation of neurotransmitter release[29].

In summary, our results indicate that Aβ43, which has largely been overlooked, is potently amyloidogenic and toxic, and highlight the potential value of Aβ43, that is, cerebrospinal fluid Aβ43 levels, as an early marker for some of the detrimental effects of aging in the adult brain. We propose that inhibition of Aβ43 generation, such as by facilitating the conversion of Aβ43 to Aβ40 in the γ-secretase complex, should be beneficial for prevention of Aβ amyloidosis.

METHODS

Methods and any associated references are available in the online version of the paper at http://www.nature.com/natureneuroscience/.

Note: Supplementary information is available on the Nature Neuroscience website.

ACKNOWLEDGMENTS

We thank M.N. Rossor (University College London) for sharing clinical information about the R278I mutation carriers, J.Q. Trojanowski and V.M.-Y. Lee (University of Pennsylvania) for providing postmortem brain tissues, R. Kopan (Washington University) for providing Myc-tagged ΔNotch1 plasmid, A. Takashima (RIKEN Brain Science Institute) for providing antibody to Aph-1, and J. Hardy (University College London) for valuable discussions. This work was supported by research grants from RIKEN Brain Science Institute, the Ministry of Education, Culture, Sports, Science and Technology, the Ministry of Health, Labor and Welfare of Japan, the TAKEDA Science Foundation, the Fund for Scientific Research – Flanders (FWO-V), the Interuniversity Attraction Poles program P6/43 of the Belgian Federal Science Policy Office and a Methusalem Excellence Grant of the Flemish Government to C.V.B. N.B receives a FWO-V postdoctoral fellowship.

AUTHOR CONTRIBUTIONS

This study was jointly designed by T. Saito, T. Suemoto and T.C.S. Experiments were performed by T. Saito, T. Suemoto, N.M., Y.M., K.Y. and S.F. T. Saito, T. Suemoto, S.F., K.Y., P.N., J.T., M.N., N.I., C.V.B., Y.I. and T.C.S. jointly analyzed and interpreted data. N.B., K.S. and C.V.B. identified pathogenic PS1 mutations in patients and families and generated *PSEN1* vector constructs for expression studies.

COMPETING FINANCIAL INTERESTS

The authors declare no competing financial interests.

Published online at http://www.nature.com/natureneuroscience/.
Reprints and permissions information is available online at http://www.nature.com/reprints/index.html.

1. Blennow, K., de Leon, M.J. & Zetterberg, H. Alzheimer's disease. *Lancet* **368**, 387–403 (2006).
2. Miravalle, L. *et al.* Amino-terminally truncated Aβ peptide species are the main component of cotton wool plaques. *Biochemistry* **44**, 10810–10821 (2005).
3. Van Vickle, G.D. *et al.* TgCRND8 amyloid precursor protein transgenic mice exhibit an altered γ-secretase processing and an aggressive, additive amyloid pathology subject to immunotherapeutic modulation. *Biochemistry* **46**, 10317–10327 (2007).
4. Iizuka, T. *et al.* Amyloid β-protein ending at Thr43 is a minor component of some diffuse plaques in the Alzheimer's disease brain, but is not found in cerebrovascular amyloid. *Brain Res.* **702**, 275–278 (1995).
5. Parvathy, S. *et al.* Correlation between Aβx-40-, Aβx-42- and Aβx-43-containing amyloid plaques and cognitive decline. *Arch. Neurol.* **58**, 2025–2032 (2001).
6. Welander, H. *et al.* Aβ43 is more frequent than Aβ40 in amyloid plaque cores from Alzheimer disease brains. *J. Neurochem.* **110**, 697–706 (2009).
7. Keller, L. *et al.* The *PSEN1* I143T mutation in a Swedish family with Alzheimer's disease: clinical report and quantification of Aβ in different brain regions. *Eur. J. Hum. Genet.* **18**, 1202–1208 (2010).
8. Qi-Takahara, Y. *et al.* Longer forms of amyloid β protein: implications for the mechanism of intramembrane cleavage by γ-secretase. *J. Neurosci.* **25**, 436–445 (2005).
9. Takami, M. *et al.* γ-Secretase: successive tripeptide and tetrapeptide release from the transmembrane domain of β-carboxyl terminal fragment. *J. Neurosci.* **29**, 13042–13052 (2009).
10. Shimojo, M. *et al.* Enzymatic characteristics of I213T mutant Presenilin-1/γ-secretase in cell models and knock-in mouse brains: FAD-linked mutation impairs γ-site cleavage of APP-CTFβ. *J. Biol. Chem.* **283**, 16488–16496 (2008).
11. Jarrett, J.T., Berger, E.P. & Lansbury, P.T. Jr. The carboxy terminus of the β amyloid protein is critical for the seeding of amyloid formation: implications for the pathogenesis of Alzheimer's disease. *Biochemistry* **32**, 4693–4697 (1993).
12. Bitan, G. *et al.* Amyloid β-protein (Aβ) assembly: Aβ40 and Aβ42 oligomerize through distinct pathways. *Proc. Natl. Acad. Sci. USA* **100**, 330–335 (2003).
13. Nakaya, Y. *et al.* Random mutagenesis of presenilin-1 identifies novel mutants exclusively generating long amyloid β-peptides. *J. Biol. Chem.* **280**, 19070–19077 (2005).
14. Godbolt, A.K. *et al.* A presenilin 1 R278I mutation presenting with language impairment. *Neurology* **63**, 1702–1704 (2004).
15. Shen, J. *et al.* Skeletal and CNS defects in Presenilin-1-deficient mice. *Cell* **89**, 629–639 (1997).
16. Wong, P.C. *et al.* Presenilin 1 is required for Notch1 and Dll1 expression in the paraxial mesoderm. *Nature* **387**, 288–292 (1997).
17. Culvenor, J.G. *et al.* Characterization of presenilin complexes from mouse and human brain using blue native gel electrophoresis reveals high expression in embryonic brain and minimal change in complex mobility with pathogenic presenilin mutations. *Eur. J. Biochem.* **271**, 375–385 (2003).
18. Evin, G. *et al.* Transition-state analogue γ-secretase inhibitors stabilize a 900 kDa presenilin/nicastrin complex. *Biochemistry* **44**, 4332–4341 (2005).
19. Thinakaran, G. *et al.* Endoproteolysis of presenilin 1 and accumulation of processed derivatives *in vivo*. *Neuron* **17**, 181–190 (1996).
20. Lee, M.K. *et al.* Hyperaccumulation of FAD-linked presenilin 1 variants *in vivo*. *Nat. Med.* **3**, 756–760 (1997).
21. Kaneko, H. *et al.* Enhanced accumulation of phosphorylated α-synuclein and elevated β-amyloid 42/40 ratio caused by expression of the presenilin-1 ΔT440 mutant associated with familial Lewy body disease and variant Alzheimer's disease. *J. Neurosci.* **27**, 13092–13097 (2007).
22. Schroeter, E.H. *et al.* A presenilin dimer at the core of the γ-secretase enzyme: insight from parallel analysis of Notch1 and APP proteolysis. *Proc. Natl. Acad. Sci. USA* **100**, 13075–13080 (2003).
23. Hama, E., Shirotani, K., Iwata, N. & Saido, T.C. Effects of neprilysin chimeric proteins targeted to subcellular compartments on amyloid β peptide clearance in primary neurons. *J. Biol. Chem.* **279**, 30259–30264 (2004).
24. Kumar-Singh, S. *et al.* Mean age-of-onset of familial Alzheimer disease caused by presenilin mutations correlates with both increased Aβ42 and decreased Aβ40. *Hum. Mutat.* **27**, 686–695 (2006).
25. Wang, R., Wang, B., He, W. & Zheng, H. Wild-type presenilin 1 protects against Alzheimer disease mutation–induced amyloid pathology. *J. Biol. Chem.* **281**, 15330–15336 (2006).
26. Maeda, J. *et al.* Longitudinal, quantitative assessment of amyloid, neuroinflammation, and anti-amyloid treatment in a living mouse model of Alzheimer's disease enabled by positron emission tomography. *J. Neurosci.* **27**, 10957–10968 (2007).

© 2011 Nature America, Inc. All rights reserved.

27. Saido, T.C. *et al.* Dominant and differential deposition of distinct β-amyloid peptide species, AßN3(pE), in senile plaques. *Neuron* **14**, 457–466 (1995).
28. Schilling, S. *et al.* Glutaminyl cyclase inhibition attenuates pyroglutamate Aβ and Alzheimer's disease–like pathology. *Nat. Med.* **14**, 1106–1111 (2008).
29. Zhang, C. *et al.* Presenilins are essential for regulating neurotransmitter release. *Nature* **460**, 632–636 (2009).
30. Russo, C. *et al.* Presenilin-1 mutations in Alzheimer's disease. *Nature* **405**, 531–532 (2000).
31. McGowan, E. *et al.* Aβ42 is essential for parenchymal and vascular amyloid deposition in mice. *Neuron* **47**, 191–199 (2005).
32. Kim, J. *et al.* Aβ40 inhibits amyloid deposition in vivo. *J. Neurosci.* **27**, 627–633 (2007).
33. Ono, K., Condron, M. & Teplow, D.B. Effects of the English (H6R) and Tottori (D7N) familial Alzheimer disease mutations on amyloid β-protein assembly and toxicity. *J. Biol. Chem.* **285**, 23186–23197 (2010).
34. Jan, A. *et al.* The ratio of monomeric to aggregated forms of Aβ40 and Aβ42 is an important determinant of amyloid-β aggregation, fibrillogenesis, and toxicity. *J. Biol. Chem.* **283**, 28176–28189 (2008).
35. Huppert, S.S. *et al.* Embryonic lethality in mice homozygous for a processing-deficient allele of Notch1. *Nature* **405**, 966–970 (2000).
36. Ikeuchi, T. *et al.* Familial Alzheimer disease-linked presenilin 1 variants enhance production of both Aβ1–40 and Aβ1–42 peptides that are only partially sensitive to a potent aspartyl protease transition state inhibitor of "γ-secretase". *J. Biol. Chem.* **278**, 7010–7018 (2003).
37. Serneels, L. *et al.* γ-Secretase heterogeneity in the Aph1 subunit: relevance for Alzheimer's disease. *Science* **324**, 639–642 (2009).
38. Bentahir, M. *et al.* Presenilin clinical mutations can affect γ-secretase activity by different mechanisms. *J. Neurochem.* **96**, 732–742 (2006).
39. Deng, Y. *et al.* Deletion of presenilin 1 hydrophilic loop sequence leads to impaired γ-secretase activity and exacerbated amyloid pathology. *J. Neurosci.* **26**, 3845–3854 (2006).
40. Hara, H. *et al.* Development of a safe oral Aβ vaccine using recombinant adeno-associated virus vector for Alzheimer's disease. *J. Alzheimers Dis.* **6**, 483–488 (2004).
41. Mouri, A. *et al.* Oral vaccination with a viral vector containing Aβ cDNA attenuates age-related Aβ accumulation and memory deficits without causing inflammation in a mouse Alzheimer model. *FASEB J.* **21**, 2135–2148 (2007).
42. Kimura, N. *et al.* Senile plaques in an aged Western Lowland Gorilla. *Exp. Anim.* **50**, 77–81 (2001).
43. Sturchler-Pierrat, C. *et al.* Two amyloid precursor protein transgenic mouse models with Alzheimer disease–like pathology. *Proc. Natl. Acad. Sci. USA* **94**, 13287–13292 (1997).
44. Huang, S.-M. *et al.* Neprilysin-sensitive synapse-associated amyloid-β peptide oligomers impair neuronal plasticity and cognitive function. *J. Biol. Chem.* **281**, 17941–17951 (2006).

© 2011 Nature America, Inc. All rights reserved.

ONLINE METHODS

Generation of PS1-R278I knock-in mice. The genomic DNA of mouse *PSEN1* was isolated from the bacterial artificial chromosome (BAC) library from the 129/Sv mouse genome, and one BAC clone that included introns 5–11 of the *PSEN1* gene was obtained (**Supplementary Fig. 1**). The fragment from the ApaI site of intron 5 to the HindIII site of intron 11 provided the basis for construction of the targeting vector. To introduce the PS1-R278I mutation, we subcloned the SmaI/BamHI fragment containing introns 7 and 8 of the *PSEN1* gene into pBluescript vector. To introduce the R278I mutation, we used 5′-GGT TGA AAC AGC TCA GGA AAT AAA TGA GAC TCT CTT TCC AGC-3′ (underlined, original G to T mutation) as our primer, using GeneEditor Mutagenesis System (Promega) according to the manufacturer's protocol. This fragment was used to replace the original sequence of the *PSEN1* gene. Finally, a *pgk-neo* gene cassette was inserted for positive selection at the EcoRI/SmaI sites located in intron 7, and a diphtheria toxin A fragment cassette was inserted for negative selection at the HindIII site in intron 11. We used the ApaI/EcoRI fragment spanning from intron 5 to intron 7 (4.3 kb) as the long arm and the BamHI/HindIII fragment spanning from intron 8 to intron 11 (3.8 kb) as the short arm of the targeting vector.

Embryonic stem cell cultures and gene-targeting experiments were carried out as described previously. Targeted embryonic stem cells were microinjected into 129/Sv blastocysts. DNA was extracted from the biopsied tail of mouse pups, and the F1 generation of the mutant animals was identified by Southern blot analysis with a 3′ external probe that was produced by PCR using 5′-AAT GGA TAA TCA GAG CCT GCC-3′ and 5′-TCC TCA CAA CTA ACT ACC CAA GG-3′ as primers.

The heterozygous mice were crossbred with EIIa-Cre transgenic mice to remove the *pgk-neo* gene, after which the generated PS1-R278I knock-in mice were backcrossed to the C57BL6/J strain. When the *pgk-neo* gene was removed by Cre excision, a short sequence ranging from the EcoRI to the SmaI sites of intron 7 was also removed. Deletion of this short sequence in intron 7 enables detection of the genotype of mutant mice. To genotype the PS1-R278I knock-in mouse, tail DNA was isolated and subjected to PCR analysis using 5′-AGT TTC AGA CCA GCC TAG GCC AC-3′ and 5′-AGG AAG GGA GAC TTG ACA GC-3′ as primers.

Other mutant mice. PS1 knockout mice and PS1-M146V knock-in mice were purchased from the Jackson Laboratory. APP23 mice carrying the human APP isoform 751 transgene harboring the Swedish mutation (K651N M652L)[45] have been described previously[46]. All animal experiments were carried out according to the RIKEN Brain Science Institute's guidelines for animal experimentation.

MEFs. MEFs were prepared from E13–14 embryos of wild-type, PS1-R278I knock-in and PS1 knockout mice, and inoculated in Dulbecco's modified Eagle medium supplemented with 10% fetal bovine serum (FBS, vol/vol). The conditioned medium and cell lysates from MEFs (passage <8) were subjected to biochemical analyses, including ELISA, native PAGE and western blotting. Transfection of the MEFs with the Myc-tagged ΔNotch construct[47] was performed using FuGENE 6 Transfection Reagent (Roche) according to the manufacturer's instructions.

Blue native-PAGE (BN-PAGE). Non-denaturing native PAGE was performed to confirm the integrity of the γ-secretase complexes[17] using the Novex Bis-Tris gel system (Invitrogen) according to the manufacturer's instructions. Samples were extracted from embryonic brains and MEFs using the sample buffer from the Novex Bis-Tris gel system that contains 1% digitonin. Equal amounts of proteins as determined using the BCA Protein Assay Kit (Pierce) were loaded on a 3–12% gradient Bis-Tris acrylamide gel. Immunoblotting was performed using the antibodies H70 (to the PS1 N terminus, Santa Cruz) and Ab-2 (to PS2, Calbiochem).

Immunoprecipitation assay and western blot analysis. Brain homogenates from embryonic brains (E14–16) and cell lysates of MEFs were immunoprecipitated with H70, and then captured by Dynabead-conjugating protein G (Invitrogen). Immunoprecipitants were subjected to western blot analysis using antibodies H70, MAB5232 (to the PS1 loop, Chemicon), Ab-2, PA1-758 (to Nicastrin, Affinity Bioreagents) and ACS-01 (to Aph1)[10], and antibody to Pen-2 (Zymed). In addition, we used antibody to Aβ1-12 (6E10, Covance), antibody to the N terminus of APP (22C11, Chemicon), antibody to APP CTF (Sigma), antibody to Myc (9B11, Cell Signaling), antibody to Notch1 (mN1A, BD Bioscience) and antibody to β-actin (AC-15, Sigma).

ELISA. Soluble materials from mouse cortical hemispheres were dissolved in Tris-HCl–buffered saline and the insoluble materials were dissolved in guanidine-HCl solution as described previously[48]. Samples from the brains and from the conditioned medium of MEFs were analyzed using an Aβ-ELISA kit (Wako) to quantify Aβ40. To specifically quantify the levels of Aβ42 and Aβ43, we established an Aβ42- and Aβ43-specific sandwich ELISA system using the Aβ-ELISA kit (Wako). Given that BC05, a detection antibody of this kit, cross-reacts with Aβ42 and Aβ43 (ref. 35), we used the Aβ42- and Aβ43-specific antibodies C42 (Aβ42 specific, IBL) and C43 (Aβ43 specific, IBL). The specificities of these antibodies are shown in **Figure 2c–e** and **Supplementary Figure 6c–e**. Samples were incubated overnight at 4 °C in a 96-well plate coated with the capture antibody, BNT77 (antibody to Aβ11–28)[49]. Aβ from samples captured in the ELISA were incubated with C42 or C43 (1:100, 3 h at 20–25 °C), after which horseradish peroxidase–conjugated antibody to rabbit IgG (1:500, 2 h at 20–25 °C) was added as a detection antibody. Synthesized Aβ42 or Aβ43 peptide (Peptide Institute) was used for the preparation of a standard curve, and diluted with the diluents solutions provided in the kit. For consistency, when we quantified the amount of Aβ40, a synthesized Aβ40 peptide (Peptide Institute) was also used for the preparation of a standard curve. This system also worked in broader concentration range of Aβ42 and Aβ43 (**Supplementary Fig. 6a,b**). Furthermore, a highly sensitive Aβ43 system, based on modified protocols, was established for the measurement of samples containing small amounts of Aβ43, such as samples derived from non–APP transgenic mice and cells that are not overexpressing APP (**Supplementary Fig. 7**).

Immunohistochemical and histochemical studies. Paraffin-embedded mouse brain sections were immunostained with 4G8 (antibody to Aβ17-24, Covance), C40 (specific antibody to Aβ40, IBL), C42, C43 and MAB3402 (antibody to GFAP, Chemicon), with or without tyramide signal amplification (PerkinElmer Life Sciences) as described previously[48]. Quantification of immunoreactivity from brain sections were carried out using MetaMorph imaging software (Universal Imaging) as previously described[48].

Y-maze test. Mice were housed individually before transferring to the behavioral laboratory. They were kept during the behavioral analysis. The light condition was 12-h:12-h (lights on 8:00). The laboratory was air-conditioned and maintained at a temperature of approximately 22–23 °C and a humidity of approximately 50–55%. Food and water were freely available except during experimentation. Large tweezers were used to handle mice to avoid individual differences in the handling procedure. All of the experiments were conducted in the light phase (9:00–18:00), and the starting time of the experiments was kept constant.

The Y-maze apparatus (O'Hara) was made of gray plastic and consisted of three compartments (3-cm (width) bottom and 10-cm (width) top, 40 cm (length) and 12 cm (height)) radiating out from the center platform (3 × 3 × 3 cm triangle). The maze was positioned 80 cm above the floor, surrounded by a number of desks and test apparatuses around the maze to act as spatial cues. In this test, each mouse was placed in the center of the maze facing toward one of the arms and was then allowed to explore freely for 5 min. Experiments were performed at a light intensity of 150 lx at the platform. An arm entry was defined as four legs entering one of the arms, and the experimenter counted the sequence of entries by watching a TV monitor behind a partition. An alternation was defined as entry into all three arms on consecutive choices (the maximum number of alternations was the total number of entries minus 2). The percent alternation was calculated as (actual alternations divided by maximum alternations) × 100. The percent alternation was designated as the spontaneous alternation behavior of the mouse, was taken as a measure of memory performance.

Thioflavin T–binding assay. The thioflavin T–binding assay was performed by mixing aliquots of Aβ. Human Aβ1–40, Aβ 1–42 and Aβ1–43 were purchased from the Peptide Institute. We first examined the aggregation properties of Aβ40, Aβ42 and Aβ43 individually by incubating the peptides separately at 20 μM in 50 mM potassium phosphate buffer (pH 7.4) at 37 °C for 24 h with agitation. The stoichiometric effect of different Aβ species on aggregation was investigated in

© 2011 Nature America, Inc. All rights reserved.

the mixture of Aβ40 and Aβ42 by adding and mixing Aβs in 50 mM potassium phosphate buffer (pH 7.4) at molar concentrations of 20:2:0.2 μM (Aβ40:Aβ42:Aβ40, Aβ42 or Aβ43 = 100:10:1) and incubating them at 37 °C for 24 h with agitation. After incubation, thioflavin T was added to a final concentration of 5 μM and thioflavin T fluorescence was measured at excitation and emission wavelengths of 442 nm and 485 nm, respectively.

Neural cell toxicity assay. Primary cortical neurons were isolated as previously described[23] and plated at a density of 5×10^4 cells per well in 96-well plate ($n = 6$ wells in each experimental conditions). We treated 10–14 d *in vitro* cultures with synthesized Aβ40, Aβ42 and Aβ43 peptide (Peptide Institute) at 0.1 to 10 μM of Aβs for 72 h. These Aβ peptides were dissolved in 10 mM phosphate buffer (pH 7.4, 90%) and 60 mM NaOH (10%), which was used as the vehicle[33]. SH-SY5Y cells were plated at a density of 2×10^4 cells per well with 10% FBS supplemented medium in 96-well plate ($n = 6$ wells in each experimental conditions), and incubated for 24 h. Then the medium was replaced with medium containing 1% FBS (vol/vol), and treated with each Aβ peptides for 48 h. Cell viability was determined using MTS assay (CellTiter 96 Aqueous One Solution Cell Proliferation Assay Kit, Promega)[50], and lactate dehydrogenase release as cell toxicity was performed using CytoTox-ONE Homogeneous Membrane Integrity Assay Kit (Promega)[33], according to the manufacturer's instructions and compared to vehicle treated cells.

Alzheimer's disease brain sections. Post-mortem Alzheimer's disease brain tissues were kindly provided by J.Q. Trojanowski and V.M.-Y. Lee (University of Pennsylvania). The tissues had been fixed with ethanol or formalin and embedded in paraffin. This study was approved by the Institutional Review Board of the RIKEN Brain Science Institute.

45. Kopan, R., Schroeter, E.H., Weintraub, H. & Nye, J.S. Signal transduction by activated mNotch: importance of proteolytic processing and its regulation by the extracellular domain. *Proc. Natl. Acad. Sci. USA* **93**, 1683–1688 (1996).
46. Iwata, N. *et al.* Presynaptic localization of neprilysin contributes to efficient clearance of amyloid-β peptide in mouse brain. *J. Neurosci.* **24**, 991–998 (2004).
47. Iwatsubo, T. *et al.* Visualization of Aβ42(43) and Aβ40 in senile plaques with end-specific Aβ monoclonals: evidence that an initially deposited species is Aβ42(43). *Neuron* **13**, 45–53 (1994).
48. Enya, M. *et al.* Appearance of sodium dodecylsulfate-stable amyloid β-protein (Aβ) dimer in the cortex during aging. *Am. J. Pathol.* **154**, 271–279 (1999).
49. Ryan, D.A., Narrow, W.C., Federoff, H.J. & Bowers, W.J. An improved method for generating consistent soluble amyloid-beta oligomer preparations for *in vitro* neurotoxicity studies. *J. Neurosci. Res.* **190**, 171–179 (2010).
50. Arango, D. *et al.* Systemic genetic study of Alzheimer disease in Latin America: mutation frequencies of the amyloid β precursor protein and presenilin gene in Colombia. *Am. J. Med. Genet.* **103**, 138–143 (2001).

© 2011 Nature America, Inc. All rights reserved.

MOLECULAR AND CELLULAR BIOLOGY, Oct. 2011, p. 4097–4106 Vol. 31, No. 19
0270-7306/11/$12.00 doi:10.1128/MCB.05189-11
Copyright © 2011, American Society for Microbiology. All Rights Reserved.

Vital Role of the Calpain-Calpastatin System for Placental-Integrity-Dependent Embryonic Survival▽†

Jiro Takano,[1] Naomi Mihira,[1] Ryo Fujioka,[1] Emi Hosoki,[1] Athar H. Chishti,[2] and Takaomi C. Saido[1]*

Laboratory for Proteolytic Neuroscience, RIKEN Brain Science Institute, Wako-shi, Saitama 351-0198, Japan,[1] and Department of Physiology, Tufts University School of Medicine, Boston, Massachusetts 02111[2]

Received 11 February 2011/Returned for modification 19 March 2011/Accepted 15 July 2011

Although the calpain-calpastatin system has been implicated in a number of pathological conditions, its normal physiological role remains largely unknown. To investigate the functions of this system, we generated conventional and conditional calpain-2 knockout mice. The conventional calpain-2 knockout embryos died around embryonic day 15, preceded by cell death associated with caspase activation and DNA fragmentation in placental trophoblasts. In contrast, conditional knockout mice in which calpain-2 is expressed in the placenta but not in the fetus were spared. These results suggest that calpain-2 contributes to trophoblast survival via suppression of caspase activation. Double-knockout mice also deficient in calpain-1 and calpastatin resulted in accelerated and rescued embryonic lethality, respectively, suggesting that calpain-1 and -2 at least in part share similar *in vivo* functions under the control of calpastatin. Triple-knockout mice exhibited early embryonic lethality, a finding consistent with the notion that this protease system is vital for embryonic survival.

The calpain-calpastatin system, ubiquitously expressed in most tissues of vertebrates, mainly consists of calpain-1, calpain-2, and calpastatin, a specific inhibitor protein that suppresses the proteolytic activity of both the isozymes (12, 34). Calpain-1 and -2 require micro- and millimolar concentrations of calcium ion, respectively, to produce a biochemical reaction *in vitro*. Calpain exists as a stoichiometric heterodimer composed of a distinct catalytic subunit with a molecular mass of ~80 kDa and an identical regulatory subunit of ~30 kDa. The catalytic subunits of calpain-1 and -2 are encoded by the genes *Capn1* and *Capn2*, respectively, whereas the regulatory subunit is encoded by *Capns1*. In general, calpain cleaves substrates at a hinge region between neighboring functional and regulatory domains, leading to activation, inactivation, or destruction of the substrate proteins. Recently, more than 10 calpain isoforms have been identified in mammals (29).

The calpain-calpastatin system has been shown to participate in a number of pathological conditions, including hypoxia, ischemia, spinal cord injury, Alzheimer's disease, muscular dystrophy, cataract, and lissencephaly (26, 36, 39). This is reflected in the finding that calpastatin deficiency enhances amyloidosis, inflammation, and neuronal atrophy in a mouse model of Alzheimer's disease (M. Higuchi and T. C. Saido, unpublished data). In contrast, the normal physiological functions of calpain remain largely unresolved, although there is indirect evidence for its involvement in cell death, differentiation, development, and memory formation (5, 6, 9). However, to date calpain activation has only been detected under pathological or artificial conditions. One intrinsic problem is the absence of a solely calpain-specific low-molecular-weight inhibitor, with most previous studies of the physiological functions of calpain relying on less-specific synthetic inhibitors, leaving open the possibility that other proteases, such as cathepsin B, H, L, S, and K, might be involved (16).

To overcome these drawbacks, genetically modified mice deficient in components of the calpain system were generated. *Capns1* deficiency led to the disappearance of both calpain-1 and -2 at the protein level, resulting in embryonic lethality around embryonic day 10.5 (E10.5) supposedly due to cardiac defects and hemorrhages (2). This provided the first indication that the calpain system is essential for embryonic development. In contrast, *Capn1* knockout (KO) mice did not show any prominent defects in fertility, development, or anatomy except for the fact that platelet aggregation and integrin β_3 phosphorylation were somewhat restricted (3). These observations surprised long-term investigators in the field, as calpain-1 had been predicted to be physiologically more important than calpain-2 based on its higher sensitivity for calcium.

The situation regarding calpain-2 remained more complex. *Capn2* KO mice were reported to die in the preimplantation stage, at E2.5 (7). However, this appeared contradictory to the phenotype of the *Capns1* KO mice, in which both calpain-1 and -2 are absent, given that the *Capns1* KO embryos died much later, at E10.5 (2). Although this discrepancy has not yet been resolved, the results suggested the relatively greater importance of calpain-2 compared to calpain-1 in physiological terms. How then can calpain-2 be activated *in vivo*? Several mechanisms were initially proposed, including autocleavage of the N-terminal regulatory domain, translocation to phospholipid membranes, and dissociation of the regulatory subunit (31). More recently, phosphorylation by extracellular signal-

* Corresponding author. Mailing address: Laboratory for Proteolytic Neuroscience, RIKEN Brain Science Institute, Wako-shi, Saitama 351-0198, Japan. Phone: 81-48-467-9715. Fax: 81-48-467-9716. E-mail: saido@brain.riken.jp.

† The authors have paid a fee to allow immediate free access to this article.

▽ Published ahead of print on 26 July 2011.

Downloaded from http://mcb.asm.org/ on February 26, 2014 by RIKAGAKU KENKYUJO (RIKEN)

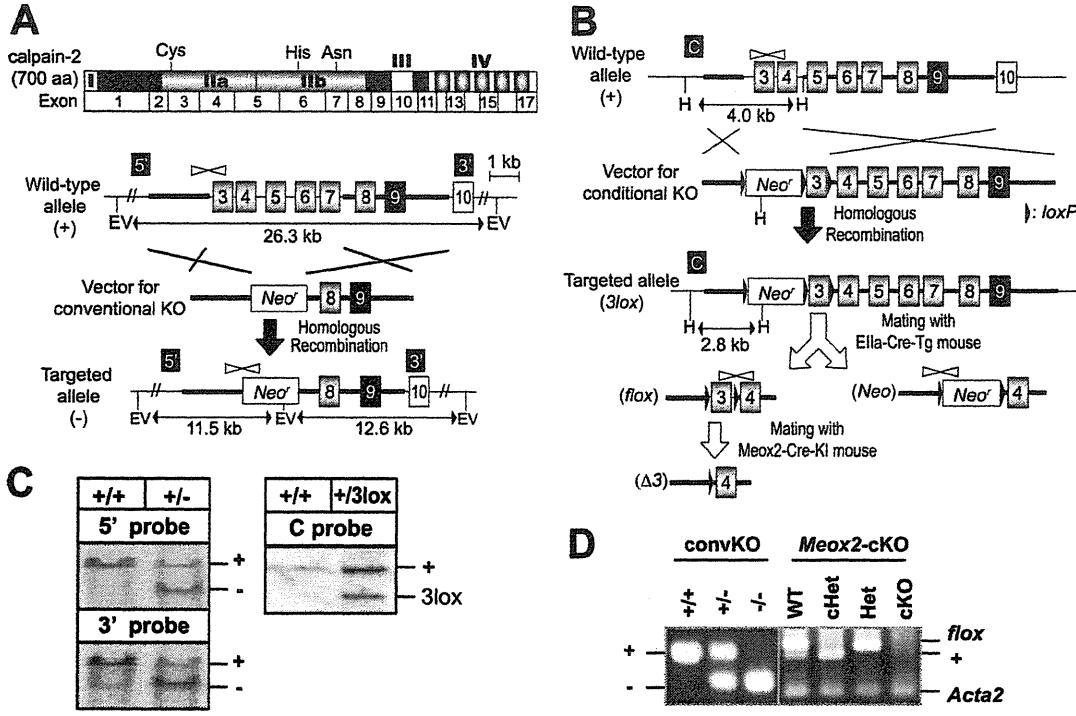

FIG. 1. Gene targeting of *Capn2* in mice. (A) Gene targeting for *Capn2* KO. Schematic representations of the domain structure of calpain-2 protein, the exon structure, the wild-type allele (+), the targeting vector for conventional *Capn2* KO, and the resultant targeted allele (−). Exons 3 to 7, including the catalytic triad (Cys105, His262, and Asn286 in protease domains IIa and IIb), were deleted in the targeted allele. The probe positions for Southern blotting (5′ and 3′ in black boxes), primer positions for *Capn2* KO PCR genotyping (white arrowheads), the homologous region with targeting vector (bold line), restriction enzyme EcoRV sites (EV), neomycin resistance gene cassette (Neo^r), and the expected sizes in Southern blotting are indicated. (B) Gene targeting for generation of the *Capn2* cKO and a second *Capn2* KO line. Schematic representations of the wild-type allele, the targeting vector for cKO, the targeted allele (*3lox*), and alleles deleted of *loxP*-flanked regions in *Cre*-transgenic mice (flox, Neo, and Δ3). By mating with *EIIa-Cre* transgenic mice (22), the *loxP*-flanked neomycin resistance gene cassette and exon 3 were removed from the (*3lox*) allele to generate the *Capn2* cKO line and another *Capn2* KO line, respectively. *Meox2-Cre* knock-in (KI) mice were mainly used for *Capn2* cKO analysis. The probe (C in black box) and restriction enzyme HindIII sites (H) for Southern blotting, primer positions for *Capn2* cKO PCR genotyping (black arrow), and *loxP* sequences (black arrowhead) are indicated. For PCR genotyping for the second *Capn2* KO line having the (Neo) allele, the same primers (see panel A) as for detection of the (−) allele were used. (C) Southern blotting to identify targeted embryonic stem cells. For the *Capn2* KO, the 11.5- and 12.6-kb genomic fragments from the (−) allele were detected with the 5′ and 3′ probes (black boxes in panel A), respectively. For the *Capn2* cKO, the 2.8-kb fragment from the (3lox) allele was detected with the C probe (black box in panel B). (D) PCR genotyping to identify mutant alleles. The left panel shows agarose gel electrophoresis of PCR products from $Capn2^{+/+}$, $Capn2^{+/-}$, and $Capn2^{-/-}$ fetuses. The right panel shows agarose gel electrophoresis of PCR products from $Meox2^{+/+}$ $Capn2^{+/flox}$ (WT), $Meox2^{Cre/+}$ $Capn2^{+/flox}$ (cHet), $Meox2^{+/+}$ $Capn2^{-/flox}$ (Het), and $Meox2^{Cre/+}$ $Capn2^{-/flox}$ (cKO) animals. In the cHet and cKO, the *flox* allele was deleted by Cre recombination.

regulated kinase (ERK) and protein kinase A has emerged as a candidate mechanism for regulating the activation status of calpain-2 (11, 28).

Another way to investigate the function of calpain is to manipulate the expression of calpastatin (*Cast*), which led us to generate *Cast* KO mice and transgenic (Tg) mice that overexpress calpastatin using the *Camk2a* promoter (17, 32). Both phenotypes were essentially normal in terms of their reproduction, development, growth, anatomy, and cognition, although the *Cast* KO mice exhibited modest abnormality in affective behavior (24). In contrast, calpastatin deficiency augmented excitotoxic neurodegeneration, which in turn was suppressed by calpastatin overexpression (17, 32). Thus, calpastatin appeared to play a more significant role under pathological rather than physiological conditions.

In summary, recent reverse genetic studies have highlighted the potential physiological importance of calpain-2. Here, we independently generated conventional and conditional *Capn2* KO mice and found that *Capn2* deficiency does not affect embryonic survival at the preimplantation stage but rather induces cell death in placental trophoblasts at later stages, followed by cardiovascular defects. However, calpain has been known as an executer of cell death, these results suggest that both calpain-1 and -2 also have a role in cell survival signaling or maintenance.

MATERIALS AND METHODS

Generation and characterization of *Capn2* conventional and conditional KO mice. The 10-kb targeting region from introns 2 to 10 of mouse calpain-2 gene was subcloned by PCR using the primers 5′-GGGTTGTGGAGCACTGCACA CTTTGTAGTTTTCCGCTGCAACCATTTGCTGTTCTCC-3′ and 5′-CTTTG CATTTGCCAAGGGGTGGGGGCCAAAAGACAGGCAGTGTGGGAAGA TGGAGC-3′ with 129/SvEv mouse strain bacterial artificial chromosome as a template. For the *Capn2* KO, exons 3 to 7 were replaced with a neomycin resistance gene cassette with phosphoglycerate kinase promoter and polyadenyl-

Downloaded from http://mcb.asm.org/ on February 26, 2014 by RIKAGAKU KENKYUJO (RIKEN)

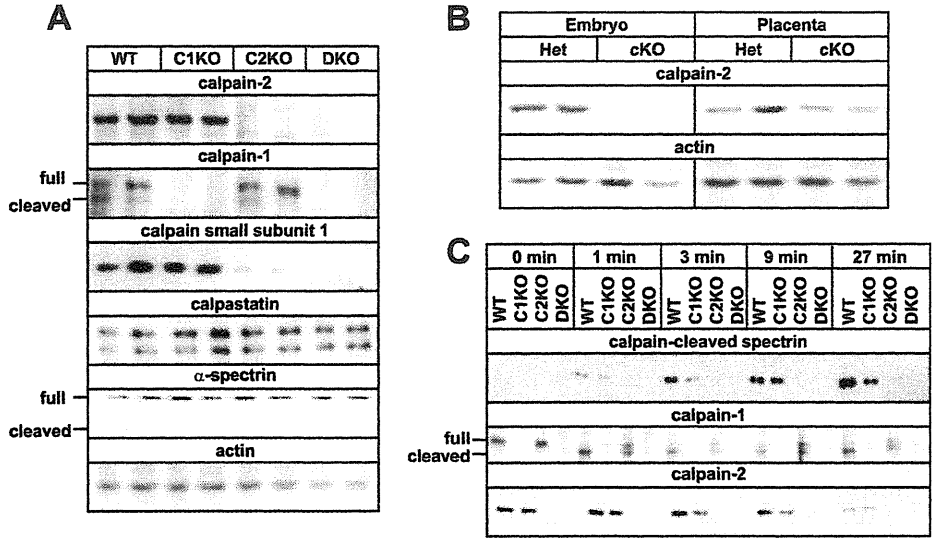

FIG. 2. Protein expressions and calpain activity. (A) Western blotting for *Capn2* conventional knockout fetuses. *Capn1*$^{+/+}$ *Capn2*$^{+/+}$ (WT), *Capn1*$^{-/-}$ *Capn2*$^{+/+}$ (C1KO), *Capn1*$^{+/+}$ *Capn2*$^{-/-}$ (C2KO), and *Capn1*$^{-/-}$ *Capn2*$^{-/-}$ (DKO) fetuses were analyzed at E10.5. Antibodies against calpain-2 domain IV, calpain-1 domain IV, calpain small subunit-1 domain VI, and calpastatin C terminus peptide were used. Using anti-calpain-1 antibody, the N-terminally autocleaved form was detected. (B) Western blotting for *Capn2* cKO from fetuses and placentas. E13.5 placentas from Het (*Meox2*$^{+/+}$ *Capn2*$^{-/flox}$) and cKO (*Meox2*$^{Cre/+}$ *Capn2*$^{-/flox}$) mice were analyzed. (C) Calpain activation assay. Calcium ion was added to brain homogenates from 3-month-old *Meox2*$^{+/+}$ *Capn1*$^{+/+}$ *Capn2*$^{+/+}$ (WT), *Meox2*$^{+/+}$ *Capn1*$^{-/-}$ *Capn2*$^{+/+}$ (C1KO), *Meox2*$^{Cre/+}$ *Capn1*$^{+/+}$ *Capn2*$^{-/flox}$ (C2cKO), and *Meox2*$^{Cre/+}$ *Capn1*$^{-/-}$ *Capn2*$^{-/flox}$ (cDKO) mice and then incubated for 0, 1, 3, 9, or 27 min at 30°C. The cleavage form of calpain-1 but not calpain-2 was detected.

ation regions to disrupt the catalytic triad of Cys105, His262, and Asn286 and make a frameshift mutation. For the *Capn2* conditional KO (cKO), exon 3 was flanked between a *loxP* sequence and a *loxP*-flanked neomycin resistance gene cassette. The targeting vectors were linearized and transfected by electroporation into embryonic stem cells derived from the 129 SvEv mouse strain.

After G418 treatment for the selection of the neomycin resistance gene-introduced clones, Southern blotting was performed to identify targeted clones using *Capn2*-specific probes, which were generated by genomic PCR using the primers 5′-TTGGAAGTCTGACAGCCAATAAAGC-3′ and 5′-TGAAGCCA GACCTGGCTTACAGTATTCC-3′ for the 5′ probe, the primers 5′-TCCTGA GATTTATACTGTGCCAGTGG-3′ and 5′-TTTAGATGGAGTGCTACTGA CAGAGG-3′ for the 3′ probe, and the primers 5′-CCCAGGTTTGGACTCAG AGACTG-3′ and 5′-TCTACATTGCATCTATGAAGATGTG-3′ for the C probe. Identified embryonic stem clones were microinjected into C57BL/6J blastocysts.

For embryonic analysis, noon of the day when a vaginal plug was recorded was considered to represent E0.5. To identify *Capn2* KOs, PCR genotyping was carried out using the three primers 5′-GAGAGTTCTGAGTTTCTCAGAGAA CGAACC-3′, 5′-AACTCCACGCCGTTCGGATGG-3′, and 5′-TGCGAGGCC AGAGGCCACTTGTGTAGC-3′. For *Capn2* cKOs, the 5′-GCTTGGCTTGCT CCTACACTCC-3′ and 5′-GCTCATCTGTGTCTCCAAAGCC-3′ primers were used with the *Acta2* primers 5′-GACAGGATGCAGAAGGAGAT-3′ and 5′-TTGCTGATCCACATCTGCTG-3′. For *Cre*-expressing mice, the 5′-CGCA GAACCTGAAGATGTTC-3′ and 5′-CGAAATCAGTGCGTTCGAAC-3′ primers were used with the *Gapdh* primers 5′-ACCACAGTCCATGCCATCA C-3′ and 5′-TCCACCACCCTGTTGCTG-3′. *EIIa-*, *Meox2-*, and *Tek-Cre* expressing mice (stock numbers 003724, 003755, and 004128, respectively) were provided by the Jackson Laboratory (20, 22, 33). Because Cre protein was expressed in germ cells under the influence of the *Meox2* promoter, *Meox2*$^{Cre/+}$ *Capn2*$^{+/-}$ males were mated to *Capn2*$^{flox/flox}$ females to generate *Capn2* cKO, Meox2$^{Cre/+}$ *Capn2*$^{-/flox}$ offspring. *Capn1* and *Cast* KO mice were as previously reported (3, 32).

Parental mice were backcrossed to C57BL/6J mice (Charles River Laboratories Japan, Inc.) over five generations. All animal experiments were carried out according to the RIKEN guidelines for animal experimentation.

Primary antibodies. Antibodies were generated against mouse calpain-2 and calpain-1 domain IV and calpain small subunit 1 domain VI, which were purified using an ImmunoPure Melon Gel IgG purification kit (Pierce) from the sera of rabbits immunized with each recombinant protein expressed in *Escherichia coli*. The anti-calpain cleaved spectrin and calpastatin antibodies were as previously generated (32). Other antibodies were purchased as indicated: α-spectrin (clone AA6; Biohit), β-actin (clone AC-15; Sigma-Aldrich), PECAM1 (clone MEC 13.3; BD Pharmingen), cytokeratin (Z0622; Dako), CD34 (MEC14.7; Abcam), smooth muscle actin (clone 1A4; Sigma-Aldrich), caspase-3 cleaved cytokeratin (M30; Roche), cleaved caspase-3 (antibody 9661; Cell Signaling Technology), cleaved caspase-8 (antibody 3259; BioVision), and cleaved caspase-9 (antibody 9504; Cell Signaling Technology).

Western blot analysis. Samples were homogenized in a 10-fold volume of 100 mM Tris-HCl (pH 7.5), 150 mM NaCl, 10 mM EDTA, 2 mM EGTA, 0.1% Triton X-100, and protease inhibitor cocktail (Roche). The techniques used for SDS-PAGE, Western blotting, immunoreactions, and detection with the ECL Advance Western blotting Kit (GE Healthcare) were as previously described (32).

For the calpain activity assay, brains were quickly frozen in liquid nitrogen and then homogenized in 20 mM Tris-HCl buffer (pH 7.5) containing 2 mM EDTA, 2 mM EGTA, 2 mM dithiothreitol, and 0.5 mg of Pefabloc (Roche)/ml, along with 0.3 μM aprotinin for serine protease inhibition, 40 μg of bestatin/ml for aminopeptidase inhibition, 1 μM pepstatin for aspartic protease inhibition, 100 nM epoxomicin for proteasome inhibition, 1× PhosSTOP phosphatase inhibitor cocktail (Roche), and 1% Triton X-100. After centrifugation at 10,000 × *g*, the supernatants were collected and incubated at 30°C after the addition of calcium chloride to a final concentration of 7 mM. The protein concentration of each sample was equalized by using BCA protein assay reagent (Pierce) to load equal amounts of samples.

Histochemistry. Mouse embryos were fixed in 4% paraformaldehyde in phosphate buffer (pH 7.3) for 24 h at 4°C. The embryos were then photographed with an Olympus SZX5 stereomicroscope. For slice staining, fixed embryos were dehydrated using an ethanol and xylene series and then embedded in paraffin blocks. The paraffin blocks were sliced at 8 μm in the case of embryos and at 4 μm for placentas. The sections were then rehydrated and stained with Mayer's hematoxylin and eosin solution (Wako Pure Chemical Industries). Immunohistochemical staining was performed by using a TSA-fluorescein system (Perkin-Elmer). To detect dead cells, an *in situ* cell death detection kit (Roche) was used with Hoechst 33342 counterstaining. Fluorescence images were acquired using a Nikon Eclipse E1000 fluorescence microscope or an Olympus FV300 confocal fluorescence microscope.

For whole-mount immunostaining, fetuses were dehydrated through a methanol series and bleached for 4 h in 5% H_2O_2 in methanol. After rehydration, the

Downloaded from http://mcb.asm.org/ on February 26, 2014 by RIKAGAKU KENKYUJO (RIKEN)

TABLE 1. Genotypes of embryos from *Capn2*$^{+/-}$ intercrosses

Age (embryonic day)	No. of embryos with genotype[a]:		
	+/+	+/−	−/−
E12.5	4	7	7
E13.5	30	42	22
E14.5	20	36	16
E15.5	30	75	2*
E16.5	25	38	2*
Adult	68	146	0*

[a] *, $P < 0.001$ (chi-square test). The embryos at E12.5, E13.5, E14.5, and E16.5 were obtained from 2, 13, 10, 8, and 4 crosses, respectively.

fetuses were washed three times with 3% skim milk–0.1% Triton X-100 in phosphate-buffered saline (PBS-MT), followed by incubation with anti-PECAM1 antibody diluted in PBS-MT. After five washes with PBS-MT, the fetuses were incubated with horseradish peroxidase-conjugated anti-rat IgG antibody (GE Healthcare), washed five times with PBS-MT, and developed with 3,3-diaminobenzidine. The reaction was stopped by rinsing the fetuses three times in PBS.

DNA laddering assay. Placentas cleaned of maternal decidua were digested with proteinase K. After removal of the protein by phenol extraction, the DNAs were precipitated with sodium chloride-containing ethanol and dissolved in 10 mM Tris-HCl (pH 8.0) and 1 mM EDTA. Then, 10 μg of DNA and 200-bp ladder marker (TaKaRa) were loaded onto a 2% agarose gel. The loaded DNA was quantified by determining the absorbance at 260 nm.

RESULTS

Generation and characterization of conventional and conditional *Capn2* knockout mice together with *Capn1 Capn2* DKO mice. To generate conventional and conditional KO mice, we designed targeting vectors for homologous recombination in embryonic stem cells to disrupt the catalytic triad region in *Capn2*, i.e., exons 3 to 7 for the KO and exon 3 for the cKO (Fig. 1A and B). We created fetal-specific cKO mice using Cre recombinase knock-in mice under the control of the *Meox2* promoter (33). *Capn1 Capn2* double KO (DKO) mice were generated by crossbreeding *Capn1* and the above *Capn2* KO mice (3). We confirmed the success of the gene targeting by Southern blotting, genomic PCR and Western blotting (Fig. 1C and D, Fig. 2A and B).

In the fetuses, calpain-2 appeared to be more abundant than

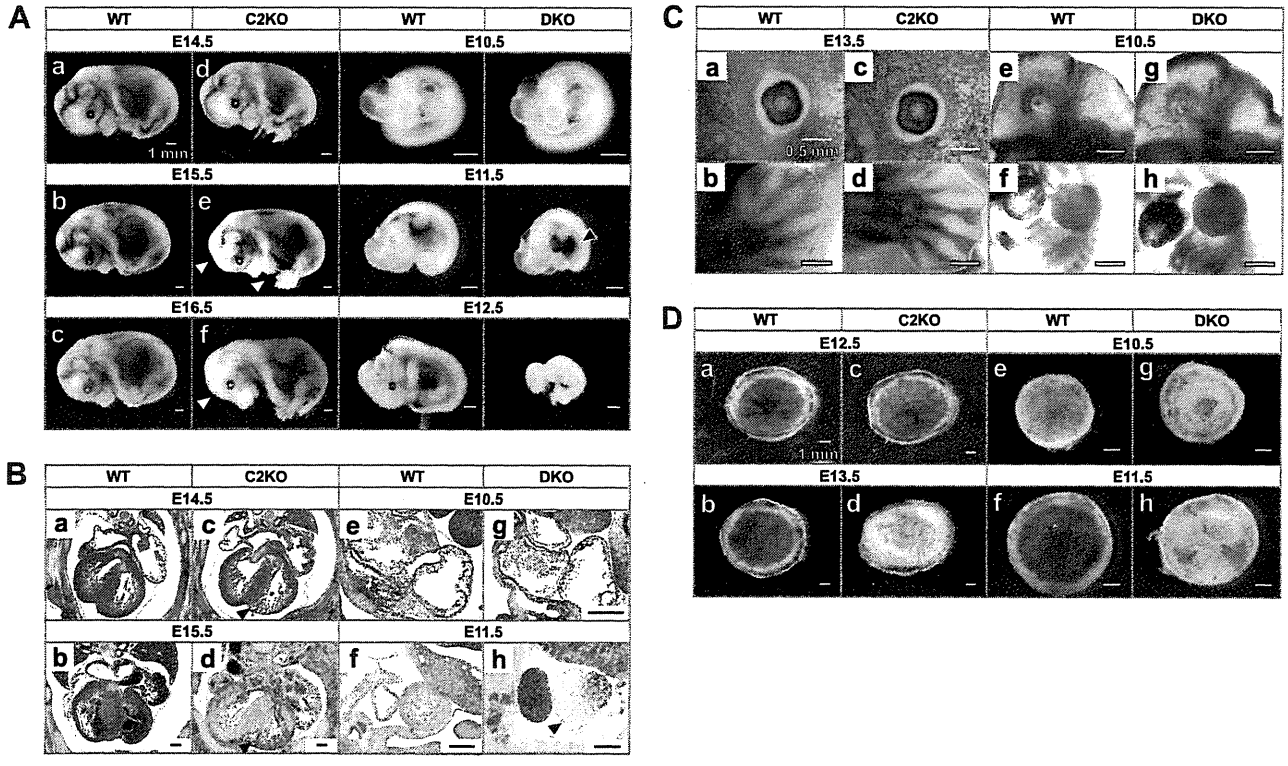

FIG. 3. *Capn2* knockout and *Capn1 Capn2* DKO embryos. (A) Appearance of mutant embryos. Wild-type (WT; a to c) and *Capn2*$^{-/-}$ embryos (C2KO; d to f) at E14.5 to E16.5 and wild-type (WT; g to i) and *Capn1*$^{-/-}$ *Capn2*$^{-/-}$ embryos (DKO; j to l) at E10.5 to E12.5 were photographed with a stereomicroscope. Peripheral vessels were diminished in six of 12 and all seven C2KO fetuses at E15.5 and E16.5, respectively (white arrowhead in panels e and f). Hepatic hemorrhages were detected in 6 of 11 DKO fetuses (black arrowhead in panel k). At E12.5 the all 14 DKO fetuses were absorbed (l). Tails were used for PCR genotyping. (B) Cardiac morphology. Transverse sections of WT (a and b) and C2KO (c and d) at E14.5 and E15.5 and sagittal sections of WT (e and f) and DKO (g and h) at E10.5 and E11.5 were stained with hematoxylin-eosin. The ventricular walls in C2KO and DKO were thinner than those of the WT (black arrowheads in panels c, d, and h). Cardiac abnormality was detected one of three and all three C2KO embryos at E14.5 and E15.5, respectively, and all three DKO embryos at E11.5. (C) Whole-mount immunostaining with anti-PECAM1 antibody. The eyes (a and c) and forelimbs (b and d) of the WT and C2KO at E13.5 and the head (e and g) and trunk (f and h) of the WT and DKO at E10.5 were visualized with diaminobenzidine after horseradish peroxidase-conjugated secondary antibody staining. We could not detected significant abnormality in all three C2KO and DKO embryos at this stage. (D) Appearance of placentas. Fetal sides of WT (a, b, e, and f), C2KO (c and d), and DKO (g and h) placentas were photographed with a stereomicroscope. Blood flow in the labyrinth was decreased in the C2KO and the DKO (d and h). We detected pale placentas (d and h) in four of 10 C2KO mice at E13.5 and all 10 DKO mice at E11.5.

Downloaded from http://mcb.asm.org/ on February 26, 2014 by RIKAGAKU KENKYUJO (RIKEN)